

# Compressive Sensing based Channel Estimation for Orthogonal Time Frequency Space (OTFS)

by

M V S Chandra Kishan  
201915003

A Thesis Submitted in Partial Fulfilment of the Requirements for the Degree of

MASTER OF TECHNOLOGY  
in  
ELECTRONICS AND COMMUNICATION

with specialization in  
Wireless Communication and Embedded Systems  
to

**DHIRUBHAI AMBANI INSTITUTE OF INFORMATION AND COMMUNICATION TECHNOLOGY**

A program jointly offered with  
**C.R.RAO ADVANCED INSTITUTE OF MATHEMATICS, STATISTICS AND COMPUTER SCIENCE**



December, 2021

## Declaration

I hereby declare that

- i) the thesis comprises of my original work towards the degree of Master of Technology in Electronics and Communications at Dhirubhai Ambani Institute of Information and Communication Technology & C.R.Rao Advanced Institute of Applied Mathematics, Statistics and Computer Science, and has not been submitted elsewhere for a degree,
- ii) due acknowledgment has been made in the text to all the reference material used.



---

M V S Chandra Kishan

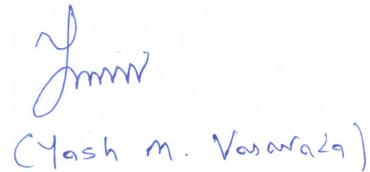
## Certificate

This is to certify that the thesis work entitled Compressive Sensing based Channel Estimation for Orthogonal Time Frequency Space (OTFS) has been carried out by M V S Chandra Kishan for the degree of Master of Technology in Electronics and Communications at *Dhirubhai Ambani Institute of Information and Communication Technology & C.R.Rao Advanced Institute of Applied Mathematics, Statistics and Computer Science* under our supervision.



---

Rajib Lochand Das  
Thesis Supervisor



---

Yash Vasavada  
Thesis Co-Supervisor

# Acknowledgments

I offer my sincere gratitude to my supervisors Prof. Rajib Lochand Das and Prof. Yash Vasavada in guideing me in the thesis work. I would like to thank Prof. Rajib for helping me in the Compressive sensing concepts whenever I was having difficulties in understanding and I was able to appreciate the concepts when applying in this work. I would like to thank Prof. Yash in helping me with the communication concepts which helped me in understanding the OTFS system model better.

# Contents

<b>Abstract</b>	<b>v</b>
<b>List of Figures</b>	<b>vi</b>
<b>1 Introduction</b>	<b>1</b>
1.1 Motivation . . . . .	1
1.2 Problem Statement . . . . .	1
1.3 Contributions . . . . .	2
1.4 Organization of the Thesis . . . . .	2
<b>2 OFDM (Orthogonal Frequency Division Multiplexing)</b>	<b>3</b>
2.1 OFDM system model . . . . .	4
2.2 OFDM advantages . . . . .	6
2.3 OFDM disadvantages . . . . .	6
<b>3 OTFS (Orthogonal Time Frequency Space)</b>	<b>7</b>
3.1 OTFS System model . . . . .	12
3.1.1 OTFS modulation . . . . .	12
3.1.2 OTFS demodulation . . . . .	14
3.2 Channel Model . . . . .	15
<b>4 Compressive sensing</b>	<b>20</b>
<b>5 Delay Doppler channel estimation</b>	<b>25</b>
<b>6 Grid Design</b>	<b>27</b>
<b>7 OTFS-MA (Multiple Access)</b>	<b>30</b>
<b>8 Results</b>	<b>32</b>
<b>9 Conclusions</b>	<b>41</b>

<b>10 Future Scope</b>	<b>42</b>
<b>References</b>	<b>43</b>
<b>Appendix A</b>	<b>45</b>
<b>Appendix B</b>	<b>47</b>

# Abstract

High speed mobility is a challenging case in wireless communication where orthogonal frequency division multiplexing (OFDM) performance degrades due to high Doppler effect. A new modulation scheme orthogonal time frequency space (OTFS) that operates in the delay-Doppler (DD) domain is proposed in the literature. Considering the sparse nature of the delay-Doppler (DD) channel, we model the estimation of the channel as a sparse signal recovery problem. To solve this problem, we use compressed sensing (CS) based estimation techniques. We apply orthogonal matching pursuit (OMP), generalized OMP (gOMP), orthogonal least square (OLS) and generalized OLS (gOLS) based algorithms for DD channel estimation. We compare the performance of the proposed CS-based estimation schemes. We analyse the performance of the CS techniques for a grid pattern which has pilot symbols embedded in the data frame. We further extended the OTFS system for multi user case and analyse the performance of the CS-based channel estimation schemes.

**Keywords:** OTFS modulation, delay-Doppler channel, compressed sensing (CS), pilot arrangement, multi-user OTFS.

# List of Figures

2.1	The orthogonal sub-carriers in frequency domain. . . . .	3
2.2	Cyclic Prefix addition in the time domain. . . . .	4
2.3	Time Frequency Domain Grid . . . . .	5
2.4	OFDM system model . . . . .	5
2.5	ICI on sub-carriers . . . . .	6
3.1	The relation between TDM FDM OTFS . . . . .	8
3.2	TDM and FDM channel symbol interactions . . . . .	9
3.3	Delay Doppler channel and symbol interactions . . . . .	9
3.4	2D basis function in delay-Doppler domain . . . . .	10
3.5	Time Frequency grid and the Delay Doppler grid. . . . .	10
3.6	The relation between different domains . . . . .	11
3.7	OTFS system model block diagram . . . . .	12
3.8	2D basis functions . . . . .	13
3.9	2-D channel in the delay Doppler domain . . . . .	17
3.10	Delay-Doppler domain channel . . . . .	17
3.11	Time-frequency domain channel . . . . .	18
4.1	Percentage of successful reconstruction by CS algorithms as a function of sparsity . . . . .	24
4.2	Time taken for successful reconstruction by CS algorithms as a function of sparsity . . . . .	24
4.3	Iterations taken for successful reconstruction by CS algorithms as a function of sparsity . . . . .	24
5.1	Matrix representation of the 2D convolution. . . . .	26
6.1	The delay-Doppler grid with the pilot symbols as well as the data symbols. . . . .	28
6.2	The delay-Doppler channel response for the grid with the pilot symbols as well as the data symbols. . . . .	28

7.1	The data grids corresponding to the 4 users in delay-Doppler domain.	31
8.1	NMSE performance of OMP, gOMP, OLS, gOLS and impulse based estimation with 16 QAM symbols as the elements of the dictionary matrix. . . . .	33
8.2	NMSE performance of OMP, gOMP, OLS, gOLS and impulse based estimation with 64 QAM symbols as the elements of the dictionary matrix. . . . .	33
8.3	NMSE performance of OMP, gOMP, OLS, gOLS and impulse based estimation with 256 QAM symbols as the elements of the dictionary matrix. . . . .	34
8.4	NMSE performance of OMP algorithm with dictionary matrix elements having modulation order (i)16, (ii)64, (iii)256 and Impulse based estimation. . . . .	34
8.5	The auto correlation of the dictionary matrix with QAM symbols at different modulation order as the elements of the matrix. . . . .	35
8.6	Iterations taken by (i) OMP (ii) gOMP (iii) OLS (iv)gOLS to converge.	35
8.7	Time taken in seconds by (i) OMP, (ii) gOMP, (iii) OLS, (iv)gOLS to converge. . . . .	36
8.8	NMSE performance of OMP, gOMP, OLS, gOLS for the new grid. .	36
8.9	BER performance of estimated channel and when the channel is known while decoding at the receiver side. . . . .	37
8.10	The grid design for the 4 users in the MA-OTFS case and each grid is of size 16x16. . . . .	38
8.11	The channel response corresponding to each individual user. . . . .	38
8.12	The channel response at the receiver side. . . . .	39
8.13	NMSE performance of 8x8 grid with 4 users with max delay and max Doppler spread of 2 . . . . .	40
8.14	NMSE performance of 8x8 grid with 4 users with max delay and max Doppler spread of 4 . . . . .	40



## CHAPTER 1

# Introduction

## 1.1 Motivation

As technologies improve, the wireless applications demand high data rates. One way to tackle this is to use large bandwidths as they increase the data rates but the drawbacks of doing this is the frequency selective fading in the wireless channels. Hence multi-carrier transmissions came into effect and out of these OFDM is most commonly used in wireless transmissions.

OFDM provides high data rates with efficient use of high bandwidths and it also combats the multi-path delay. It has been deployed in the fourth-generation cellular communications.

Over the past years, interest has turned to the development of fifth-generation cellular communications [1]. It is anticipated that carrier investment will require new applications (beyond high-speed video connections), including Internet of things (IoT), and high-velocity V2X (vehicle to vehicle V2V and vehicle to infrastructure V2I) connections.

OTFS is a recent modulation technique that has been shown to have robust performance in high mobility environment [2][3][4][5]. OTFS modulation represents the channel and the information in the delay-Doppler (DD) domain rather than the time-frequency (TF) domain as done by the conventional modulation techniques. The advantage of the DD representation is that the channel is time invariant in DD domain[4].

## 1.2 Problem Statement

The delay Doppler representation of the channel used in the OTFS system is sparse in nature[2]. Due to this sparse nature we propose to use CS algorithms for estimating the channel. CS algorithms estimate the non zero elements of the DD channel and hence less parameters have to be estimated at the receiver side.

## 1.3 Contributions

The detection of the OTFS signals using the message passing is presented in [6] where the algorithm assumes the perfect knowledge of the channel at the receiver for signal detection. A channel estimation technique using impulses in the DD domain as the pilots also has been reported in [1]. The idea of embedding impulses as pilots surrounded by guard band along with the data symbols in the DD plane has been proposed in [7]. The drawback of this method is that the spectral efficiency is reduced with the inclusion of guard bands. In the current literature on OTFS the sparse nature of the delay Doppler channel is not explored while estimating.

This thesis will address the issue of estimating the DD channel using CS algorithms for OTFS system as well as multiple access OTFS (MA-OTFS) system.

## 1.4 Organization of the Thesis

In Chapter 2 we discuss the basic OFDM principles its advantages and disadvantages and Chapter 3 introduces the OTFS principles where we will discuss the transition from the TF domain to the DD domain. Then we will discuss the OTFS system model and the DD channel and address the problem of DD channel estimation. In Chapter 4 we present orthogonal matching pursuit (OMP), generalized OMP (gOMP), orthogonal least square (OLS) and generalized OLS (gOLS) based algorithms.

In Chapter 5 we modify the OTFS system equations in order to apply the CS algorithms for estimating the DD channel. In Chapter 6 we design the DD grid consisting of both the pilot and data symbols and apply the CS algorithm. Chapter 7 introduces the multiple access OTFS (MA-OTFS) system where we will discuss the grid design for using the CS-based estimation schemes. The results are presented in Chapter 8 where we compare the performance of the proposed CS-based estimation schemes with the existing impulse based channel estimation with the existing impulse based channel estimation. This is followed by the comparison of the performance of the CS algorithms for grid discussed in Chapter 6 as well as the MA-OTFS system. Lastly, Chapter 9 and Chapter 10 deal with the conclusion and the future scope in this area.

## CHAPTER 2

# OFDM (Orthogonal Frequency Division Multiplexing)

OFDM is a multi-carrier modulation scheme where the information symbols are transmitted on sub-carriers which use frequency division multiplexing. These sub-carriers are arranged such a way that they are orthogonal to each other i.e., peak of one sub-carrier is located at the zero crossing points of the remaining sub-carriers.

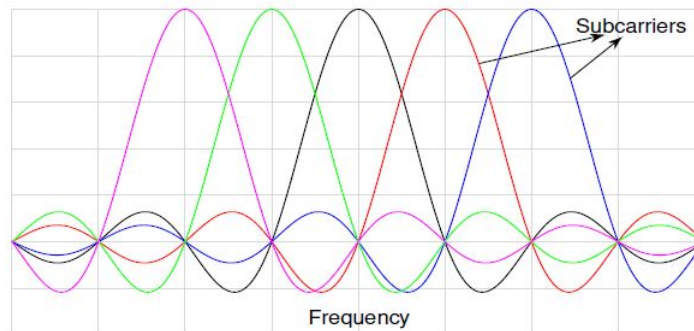


Figure 2.1: The orthogonal sub-carriers in frequency domain.

Initially at the transmitter and the receiver a large number of sub-carrier oscillators were used to do the frequency division multiplexing. The usage of discrete time Fourier transform (DFT) by Weinstein and Ebert to perform the base band modulation and demodulation eliminated the need of the bank of sub-carrier oscillators there by making the implementation of the system more efficient.

At the transmitted side the data symbols are mapped onto the sub-carriers in parallel using the IDFT (inverse discrete time Fourier transform) block. By doing this our data symbols in the frequency domain are converted to the time domain for the transmission over the channel and at the receiver the inverse operations are performed to get the received data symbols back to the frequency domain. Fast Fourier transform (FFT) and inverse fast Fourier transform (IFFT) blocks replaced

the DFT and IDFT blocks

In order to combat ISI (inter symbol interference) guard bands were used in the frequency domain and raised cosine windowing is used in the time domain to combat ICI (inter carrier interference).

With the introduction of the cycle prefix (CP) where they placed a cyclic extension of the OFDM symbol instead of using the guard band in the frequency domain this can be seen in the below Fig. 2.2. This converted the transmission over the channel as a cyclic convolution operation. Introducing the CP helps in maintaining orthogonality even in poor transmission conditions thereby removing the effect of ISI.

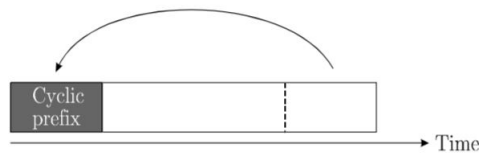


Figure 2.2: Cyclic Prefix addition in the time domain.

The orthogonality of a signal is jeopardized when it is passing through a time-dispersive channel. By introducing CP, the orthogonality between the sub-carriers is maintained and the length of the CP (or the interval occupied by the CP) should be larger than the maximum delay spread of the channel. CP ensures that the delayed replicas of the OFDM symbols will always have a complete symbol within the FFT interval (often referred as FFT window) making the transmitted signal periodic. When IFFT is taken for an OFDM symbol period the output is periodic, hence all the resulting components of the original signal are orthogonal to each other. In general, in the OFDM system can be viewed as transmitting the data on time-frequency grid. The time frequency grid can be interpreted as a sequence of  $N$  multi-carrier symbols having a spacing of  $\tau_0$  and each having  $M$  sub-carriers and having a spacing of  $\nu_0$ . The parameter  $\tau_0$  is the multi-carrier symbol duration and the parameter  $\nu_0$  is the sub-carrier spacing. We note that the bandwidth of the transmission  $B = M\nu_0$ .

## 2.1 OFDM system model

The OFDM system model is shown in Fig. 2.4, where the serial input bit stream is modulated by the modulator block and is then converted into parallel so that it can be fed into the IFFT block. By doing this the data in frequency domain

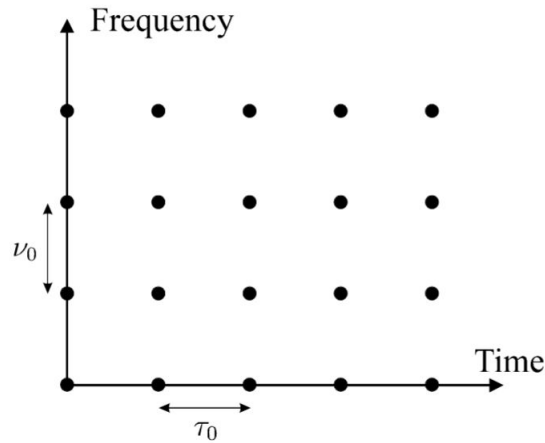


Figure 2.3: The time frequency domain grid.

is converted into time domain for transmission as discussed previously. CP is added to this in order to combat channel conditions but before adding CP the data in parallel is converted into series. The signal in discrete domain is converted into continuous domain using digital to analog converter (DAC). Now the analog signal is transmitted over the channel.

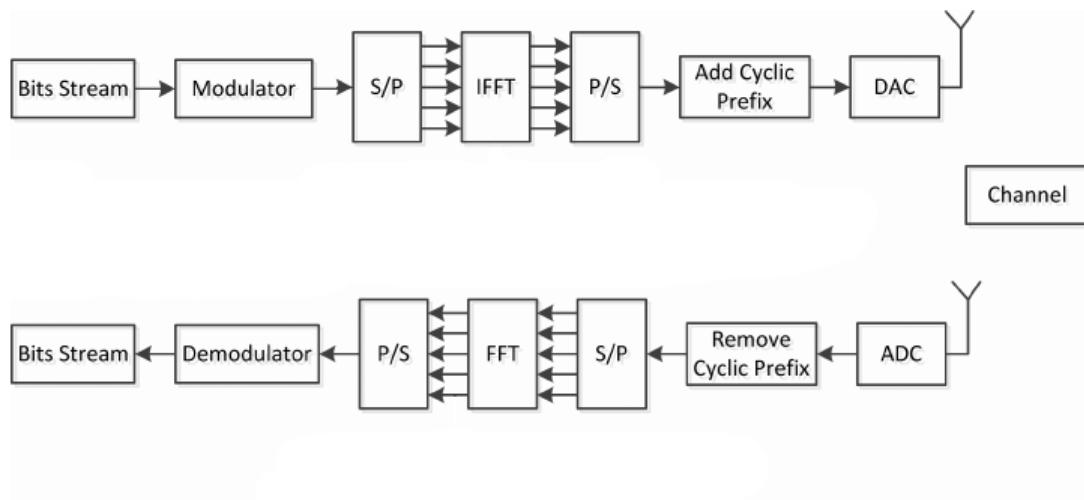


Figure 2.4: OFDM system model.

At the receiver the opposite operations are done i.e., the received analog signal is converted into the discrete signal using ADC (Analog to Digital Converter). CP is removed from this discrete signal and then further converted into parallel using serial to parallel converter block. This parallel data is fed to the FFT block which converts the time domain signal into the frequency domain signal for demodulation. The output from the FFT block is parallel which is converted into serial data and is then demodulated into the serial output bit stream.

## 2.2 OFDM advantages

- OFDM systems are more resistant to frequency selective fading when compared to the single carrier system because the channel is divided into multiple narrow sub-bands which undergo flat fading.
- The ISI is completely eliminated due to the introduction of cyclic prefix.
- The OFDM system is easy to implement due to the use of FFT techniques at the transmitter and the receiver.
- The available spectrum is effectively utilized due to the closed space overlapping of the sub-carriers.
- Channel equalization becomes simpler as it is to be applied on the sub channel instead of applying across the entire channel.

## 2.3 OFDM disadvantages

OFDM has high PAPR (Peak to Average Power Ratio) which impacts the RF amplifier efficiency as the amplifier has to be in a linear range and accommodate high amplitude variations. One of the major disadvantages of OFDM is the sensitivity to the carrier frequency offset as even a slight change in the frequency of one sub-carrier results in the loss of the orthogonality among the entire sub-carriers this results in the ICI. The loss of orthogonality among the sub-carriers is shown in Fig. 2.5

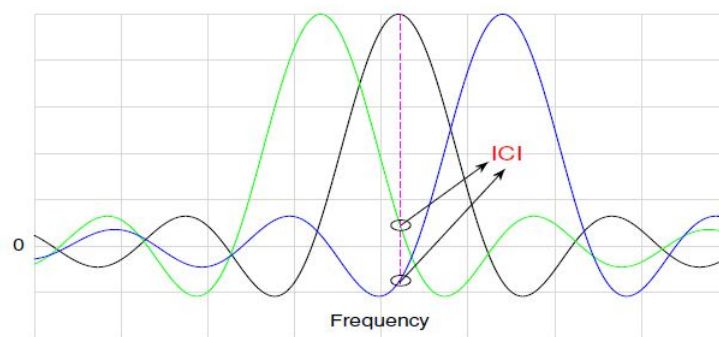


Figure 2.5: Effect of Doppler frequency on the sub-carriers.

Though this can be mitigated to some extent using the frequency-controlled oscillator but at high Doppler frequency resulting from high V2X (vehicle-to-vehicle V2V and vehicle-to-infrastructure V2I) connections, the frequency offset is so high that it is beyond the scope of FCO.

## CHAPTER 3

# OTFS (Orthogonal Time Frequency Space)

The traditional OFDM suffers performance degradation in the high Doppler conditions. One way to overcome this problem without sacrificing the performance is to combine the principles of CDMA and OFDM i.e., to combine the principle of spreading so as to have resilience to narrow band interference and the principle of orthogonality so as to simplify the channel coupling for achieving high spectral densities with better performance-complexity trade off [4].

OTFS is one such modulation scheme where the QAM data symbols are transmitted over waveforms which are spread in both the time and the frequency domains at the same time remaining orthogonal to each other. In general, OTFS combines the reliability and robustness of the spread spectrum and the high spectral efficiency low complexity of the narrow-band transmission.

For a better understanding of OTFS we look into the basic signal representation in the time and frequency domain. In the time domain representation, the signal is realized as the superimposition of the delta functions and in the frequency domain representation, the signal is the superimposition of the complex exponentials. These two representations are interchanged using the Fourier transform.

This complementary nature of the time and frequency representation is expressed by the Heisenberg uncertainty principle which states that the signal cannot be localized in both time and frequency simultaneously. Which means that if the signal is localized in the time domain, then its non-localized in the frequency domain and vice versa.

Using ZAK representation/transform a time domain signal which is neither time-limited nor bandwidth limited can be transformed into delay-Doppler domain in which the signal is localized [8]. A signal can be represented in three fundamental ways. First, it can be represented as a function of time. Second, it can be represented as a function of frequency. Third, it can be represented as function of delay and Doppler.

Similar to Fourier transform, any signal in time domain or frequency domain

can be transformed to delay-Doppler domain using Zak transform[8].

Converting the Time Domain Multiplex (TDM) pulse to the delay-Doppler representation results in a function which is localized in the delay domain but it is non localized in the Doppler domain and similar is the case when Frequency Domain Multiplex (FDM) pulse is converted to the delay-Doppler representation results in a function which is localized in the Doppler domain but it is non localized in the delay domain. A modulation based on symmetrically localized signal in the delay-Doppler representation as shown in the below Fig. 3.1 is referred to OTFS or orthogonal time frequency space.

A wireless channel is modeled as the collection of reflectors which can either be stationary or are moving. The transmitted wave is reflected by a reflector has a shift in frequency due to the relative velocity between the reflector and the receiver/transmitter and these reflections arrive at the receiver with some delay. There will also be a change in the amplitude based on the constructive or destructive interference due to numerous reflectors sharing the same properties of delay and Doppler. We now look how the channel effects the three signals discussed above i.e., the TDM, FDM and the OTFS waveforms.

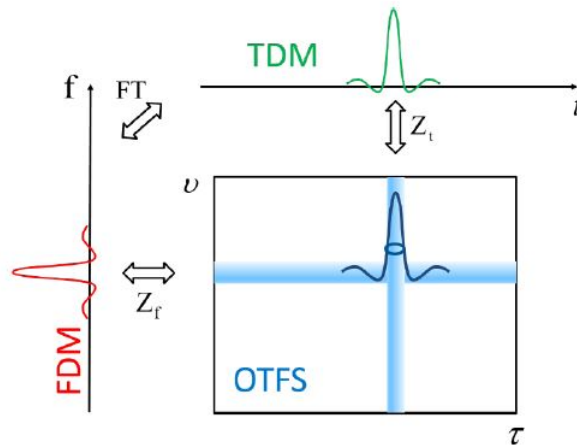


Figure 3.1: The relation between TDM FDM OTFS

In Fig. 3.2 there are 5 reflectors out of which 3 are stationary and 2 are in motion. By transmitting a localized TDM pulse we can separate the reflections of each reflector based on the delays but when reflectors have same delay but different Dopplers they are superimposed on each other and hence can't be separated. This can be seen in the Fig. 3.2 where the TDM reflections from left to right, the first and third reflections are time invariant as they are stationary, the last reflection is time variant as its moving and lastly the second reflection is the superimposition of the two reflectors where one is stationary while the other is



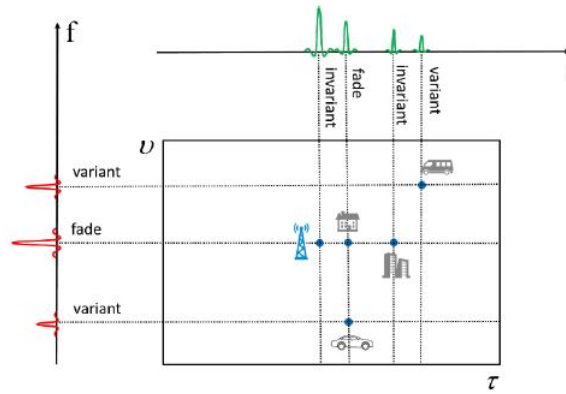


Figure 3.2: TDM and FDM channel symbol interactions

moving.

By transmitting FDM pulse we can separate the reflections of each reflector based on the Doppler values but when reflectors have same Dopplers but different delays they are superimposed on each other and hence can't be separated. This can be seen in the Fig. 3.2 where considering the FDM reflections from top to bottom the first and last reflections have different frequencies as they are moving at different velocities. The middle reflection is due to the superposition of the static reflectors.

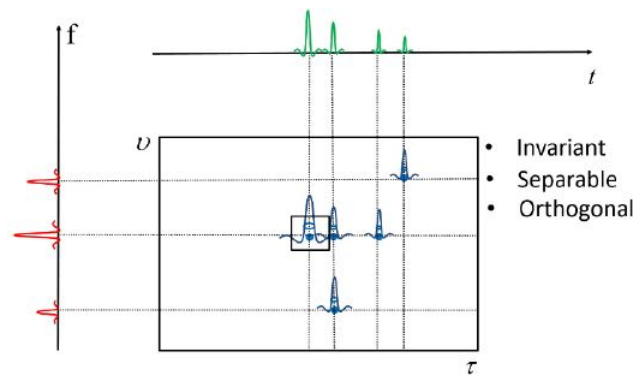


Figure 3.3: Delay Doppler channel and symbol interactions

When we transmit a localized OTFS pulse in the delay-Doppler channel we have the reflections with specific delay-Doppler shifts induced by different reflectors as shown in Fig. 3.3. The phase and the amplitude of the delay-Doppler reflections are independent of the location of the initial pulse in the domain. These reflections are also easily separated based on the delay and Doppler values, hence there is no interference and no loss of energy. These reflections are also orthogonal to each other.

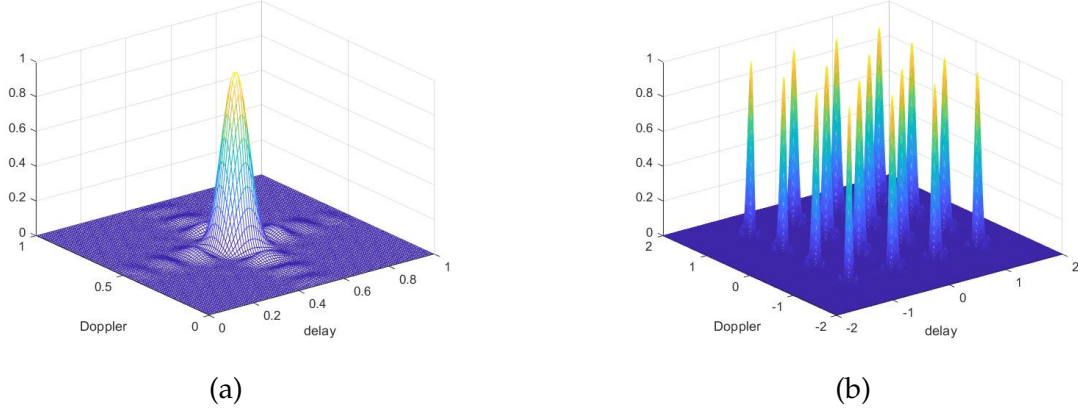


Figure 3.4: 2D basis function in delay-Doppler domain

OTFS is a time-frequency spreading scheme which are a collection of 2D basis functions defined over a time-frequency grid. OTFS is designed as a pre-processing block for the multi-carrier modulation schemes like the OFDM. This is based on the duality of the Fourier duality between the delay-Doppler and the time frequency grids.

The 2D basis signal in the delay-Doppler domain are shown in Fig. 3.4a. Each basis in Fig. 3.4b are separated by a distance of  $\frac{1}{NT}$  along the Doppler domain and a distance of  $\frac{1}{M\Delta f}$  along delay domain. Hence in a given grid there are a total of  $MN$  different basis signals which are orthogonal to each other[8].

The delay Doppler grid consists of  $M$  points along the delay axis of spacing of  $\Delta\tau = \frac{\tau}{M}$  and  $N$  points along the Doppler axis with spacing of  $\Delta\nu = \frac{\nu}{N}$  and the time-frequency grid consists of  $M$  points along the frequency axis with spacing  $\Delta f$  and  $N$  points along the time axis with a spacing of  $T$ . The time frequency grid is interpreted as a sequence of  $N$  multi-carrier symbols each having  $M$  sub-carriers. The parameter  $T$  is the multi-carrier symbol duration and the parameter  $\Delta f$  the sub-carrier spacing. We note that the bandwidth of the transmission  $B = M\Delta f$  is inversely proportional to the delay resolution  $\Delta\tau$  and the duration of the transmission  $NT$  is inversely proportional to the Doppler resolution  $\Delta\nu$ . Both the grids are presented in Fig. 3.5.

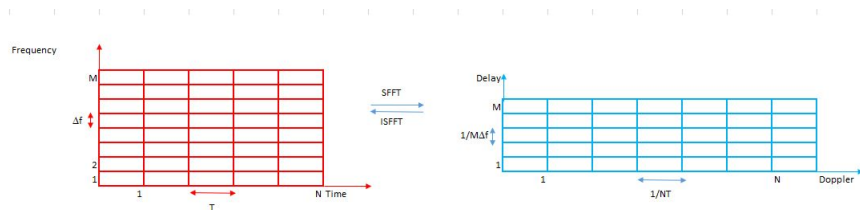


Figure 3.5: Time Frequency grid and the Delay Doppler grid.

The Fourier relation between the two grids is a variant of the 2D FFT called as symplectic finite Fourier transform (SFFT). SFFT transforms the time frequency domain into the delay-Doppler domain or the inverse symplectic finite Fourier transform (ISFFT) transforms the delay-Doppler domain to time-frequency domain which is shown in the below equation.

$$X[n, m] = \frac{1}{\sqrt{NM}} \sum_{n=0}^{N-1} \sum_{m=0}^{M-1} x[k, l] e^{j2\pi(\frac{nk}{N} - \frac{ml}{M})} \quad (3.1)$$

ISFFT can be seen as applying an M-dimensional FFT along the columns of the delay-Doppler matrix  $x[k, l]$  followed by applying N-dimensional IFFT along the rows of the matrix to get the time-frequency domain  $X[n, m]$ .

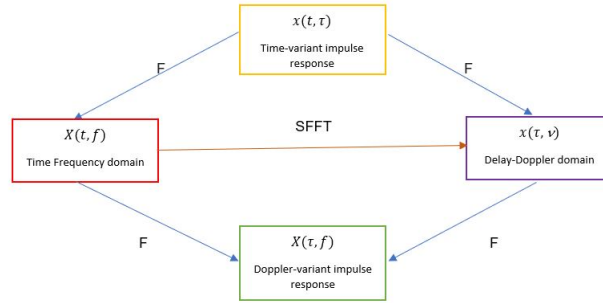


Figure 3.6: The relation between different domains

Fig. 3.6 shows the different linear time variant (LTI) wireless channels and relation between each of them.  $X(t, f)$  represents the time-frequency response,  $x(\tau, t)$  represents the time-variant impulse response,  $X(\tau, f)$  represents the Doppler-variant transfer response and  $x(\tau, \nu)$  represents the delay-Doppler response. Each response can be transformed into another by means of Fourier transform as shown in the figure.  $x[k, l]$  is the discrete delay-Doppler signal and  $X[n, m]$  is the discrete time-frequency signal.

### 3.1 OTFS System model

In this section we derive the input output relation of the OTFS mod/demod for delay-Doppler channel. Delay-Doppler plane is discretized to an information grid  $\Gamma = \{(\frac{k}{NT}, \frac{l}{M\Delta f}), k = 0, 1, \dots, N - 1, l = 0, 1, \dots, M - 1\}$  where  $\frac{1}{M\Delta f}$  and  $\frac{1}{NT}$  represent the quantization steps of delay and Doppler frequencies.

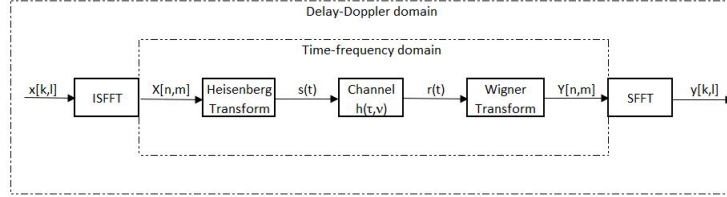


Figure 3.7: OTFS system model block diagram

First, we map the information symbols onto the delay-Doppler domain  $x [k,l]$ . The symbols in the delay-Doppler domain are converted into the time domain signal. The obtained time domain signal is then transmitted over the delay-Doppler domain channel by the transmitter. At the receiver side the received time domain signal is transformed back into the delay-Doppler domain.

#### 3.1.1 OTFS modulation

Consider a set of information symbols  $x [k, l]$   $k=0, 1, \dots, N-1, l=0, 1, \dots, M-1$  which are arranged on the delay Doppler grid. Now these symbols in the delay-Doppler domain are mapped to  $X [n, m]$   $n=0, 1, \dots, N-1, m=0, 1, \dots, M-1$  in the time frequency domain.

This is done by applying ISFFT on  $x [k, l]$  as shown in (3.1). ISFFT can be seen as applying inverse Fourier transform in Doppler domain and applying Fourier transform in the delay domain to map the symbols into time frequency domain.

In Fig. 3.8 each element of the delay-Doppler domain grid when transformed to time frequency domain spreads across the whole grid forming 2D wave forms which are orthogonal to each other. This is similar to OFDM where the data grid is mapped onto orthogonal sub-carriers, in OTFS the data grid is mapped onto the 2D orthogonal wave forms. The spreading nature of OTFS is also similar to that of CDMA.

The 2D symbols  $X[n, m]$  in time frequency domain are mapped to continuous

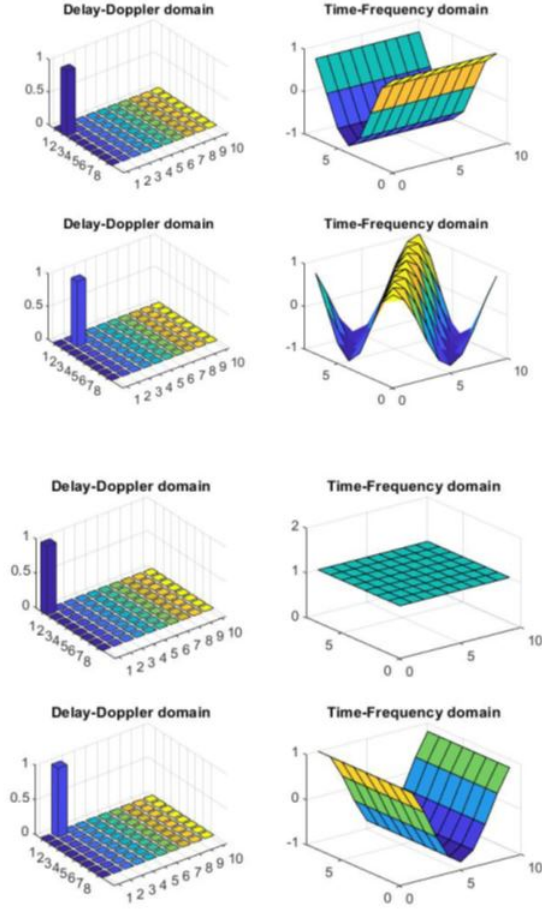


Figure 3.8: The 2D basis functions in the Information (delay-Doppler) domain (left), and the corresponding symplectic Fourier dual basis functions in the time frequency domain (right).

time domain signal  $s(t)$  as

$$s(t) = \sum_{n=0}^{N-1} \sum_{m=0}^{M-1} X[n, m] g_{tx}(t - nT) e^{j2\pi\Delta f(t-nT)} \quad (3.2)$$

The above equation is also referred to as the Heisenberg transform, where it maps the 2D symbols  $X[n, m]$  to a waveform  $s(t)$  via superimposition of delay-and-modulate operations on the pulse waveform  $g_{tx}(t)$ .

The signal  $s(t)$  is transmitted over a time-varying channel with complex base-band channel impulse response  $h(\tau, \nu)$ . The received signal  $r(t)$  is given by (neglecting the noise component in order to simplify the notations)

$$r(t) = \int \int h(\tau, \nu) s(t - \tau) e^{-j2\pi\nu(t-\tau)} d\tau d\nu \quad (3.3)$$

The transmitted signal is reflected by different reflectors and these reflections are

superposed at the receiver. Each reflection is the delayed and frequency shifted version of the transmitted signal  $s(t)$  weighted by  $h(\tau, \nu)$ . The  $\tau$  and  $\nu$  correspond to the path delay and Doppler shift introduced by the reflector.

$$h(\tau, \nu) = \sum_{i=1}^P h_i \delta(\tau - \tau_i) \delta(\nu - \nu_i) \quad (3.4)$$

3.4 is the delay-Doppler channel where  $P$  is the number of propagation paths and  $h_i, \tau_i, \nu_i$  represent the path gain, delay, and Doppler shift (or frequency) associated with  $i$ -th path, respectively, and  $\delta(\cdot)$  denotes the Dirac delta function.

### 3.1.2 OTFS demodulation

At the receiver side we perform the Wigner transform which can be seen as an inverse operation of the Heisenberg transform.

$$Y(t, f) = A_{g_{rx}, r}(t, f) = \int g_{rx}^*(t' - t) r(t') e^{-j2\pi f(t' - t)} dt' \quad (3.5)$$

Sampling the continuous signal at every  $T$  intervals in the time domain and  $\Delta f$  intervals in the frequency domain yields  $Y[n, m] = Y(t, f)|_{t=nT, f=m\Delta f}$ .

we characterize the relationship between time-frequency output samples  $Y[n, m]$  and input samples  $X[n, m]$  as

$$Y[n, m] = \sum_{n'=0}^{N-1} \sum_{m'=0}^{M-1} H_{n,m}[n', m'] X_{n,m}[n', m'] \quad (3.6)$$

Where

$$H_{n,m}[n', m'] = \int \int h(\tau, \nu) A_{g_{rx}, g_{tx}}((n - n')T - \tau, (m - m')\Delta f - \nu) e^{j2\pi(\nu + m'\Delta f)((n - n')T - \tau)} e^{j2\pi\nu n'T} d\tau d\nu \quad (3.7)$$

$H_{n,m}[n', m']$  denotes the channel in the time-frequency domain as shown in [6]. The  $g_{rx}(t), g_{tx}(t)$  pulses are said to be ideal if they satisfy the bi-orthogonal property [6].

$$\begin{aligned} A_{g_{rx}, g_{tx}}(t, f)|_{t=nT + (-\tau_{max}, \tau_{max}), f=m\Delta f + (-\nu_{max}, \nu_{max})} \\ = \delta[n] \delta[m] q_{\tau_{max}}(t) q_{\nu_{max}}(f) \end{aligned} \quad (3.8)$$

The right-hand side of (3.8) is non zero only when  $n$  and  $m$  are zeros. Substituting this in (3.7),  $H_{n,m}[n', m']$  is non zero only when  $n' = n$  and  $m' = m$ .

$$Y[n, m] = H_{n,m}[n, m]X[n, m] \quad (3.9)$$

Where

$$H_{n,m}[n, m] = \int \int h(\tau, \nu) e^{-j2\pi(\nu+m\Delta f)\tau} e^{j2\pi\nu nT} d\tau d\nu \quad (3.10)$$

The time frequency domain samples  $Y[n, m]$  are converted into the delay-Doppler domain samples  $y[k, l]$  by applying the SFFT operation.

$$y[k, l] = \frac{1}{\sqrt{NM}} \sum_{n=0}^{N-1} \sum_{m=0}^{M-1} Y[n, m] e^{-j2\pi(\frac{nk}{N} - \frac{ml}{M})} \quad (3.11)$$

The above equations can be represented as matrix equations for easy implementation at the transmitter and the receiver. (3.1) is the ISFFT operation and can be represented as matrix equation with the help of the DFT matrix i.e.,  $F_M$  and  $F_N$  which are the  $M$  point and  $N$  point DFT matrices.

$$X = F_M x F_N^H$$

Similarly, (3.2) is written as matrix equation  $S = G_{tx} F_M^H X$  and is further simplified as  $S = G_{tx} F_M^H F_M x F_N^H$ . The vectorised form of  $S$  is  $s = \text{Vec}(S) = \text{Vec}(G_{tx} x F_N^H) = (F_N^H \otimes G_{tx}) x_{lin}$ . Here  $x_{lin}$  is the vectorised version of the  $M \times N$  delay Doppler matrix  $x$ .

$$s = (F_N^H \otimes G_{tx}) x_{lin} \quad (3.12)$$

At the receiver side (3.5) can be written as  $Y = F_M G_{rx} R$  where  $R$  is the matrix form of the received vector  $r$ . Applying SFFT as shown in (3.11) we get  $y = F_M^H Y F_N$  which simplifies to  $y = G_{rx} R F_N$ . We vectorise  $y$  as  $y_{lin}$  and  $R$  as  $r$  then we get the matrix equation as

$$y_{lin} = (F_N \otimes G_{rx}) r \quad (3.13)$$

Now that we discussed on the OTFS transmitter and the receiver we look into the channel model in the delay-Doppler domain in the next chapter.

## 3.2 Channel Model

In order to obtain the channel in delay Doppler domain we simplify the end-to-end input output relation of the OTFS system in the delay-Doppler domain [6].

$$y[k, l] = \frac{1}{NM} \sum_{k'=0}^{N-1} \sum_{l'=0}^{M-1} x[k', l'] h_w[(k - k')_N, (l - l')_N] \quad (3.14)$$

where  $(*)_N$  is the modulo N operation and

$$h_w[(k - k')_M, (l - l')_N] = h_w(v, \tau) \Big|_{v=\frac{k-k'}{NT}, \tau=\frac{l-l'}{M\Delta f}}$$

$$h_w(v, \tau) = \int \int h(\tau', v') w(v - v', \tau - \tau') e^{-j2\pi v' \tau'} d\tau' dv' \quad (3.15)$$

Proof is given in Appendix A.

Substituting (3.4) we further simplify  $h_w(v, \tau)$

$$h_w(v, \tau) = \sum_{i=1}^P h_i e^{-j2\pi v_i \tau_i} w(v - v_i, \tau - \tau_i)$$

$$h_w(v, \tau) = \sum_{i=1}^P h_i e^{-j2\pi v_i \tau_i} G(v, v_i) F(\tau, \tau_i) \quad (3.16)$$

Where

$$F(\tau, \tau_i) = \sum_{m'=0}^{M-1} e^{j2\pi(\tau - \tau_i)m' \Delta f}$$

$$G(v, v_i) = \sum_{n'=0}^{N-1} e^{j2\pi(v - v_i)n' T}$$

Evaluating  $G(v, v_i)$  and  $F(\tau, \tau_i)$  at  $v = \frac{k-k'}{NT}$ ,  $\tau = \frac{l-l'}{M\Delta f}$  we get

$$F\left(\frac{l-l'}{M\Delta f}, \tau_i\right) = \sum_{m'=0}^{M-1} e^{j2\pi(l-l'-l_{\tau_i})m'} \quad (3.17)$$

$$G\left(\frac{k-k'}{NT}, v_i\right) = \sum_{n'=0}^{N-1} e^{j2\pi(k-k'-k_{v_i})n'} \quad (3.18)$$

To get the delay-Doppler channel we use (3.16), (3.17), (3.18) and for which we need the delay-Doppler coefficients and the channel coefficients as the inputs and upon substituting these values in the equations we get the 2D  $M \times N$  channel matrix in the delay-Doppler domain.

Fig. 3.9 shows the delay-Doppler channel, the non-zero elements correspond to the reflectors and their coordinates on the grid corresponds to the delay and Doppler values, the magnitude signifies the attenuation of the corresponding reflector. Since the reflectors are few in number the delay-Doppler channel is sparse in nature.



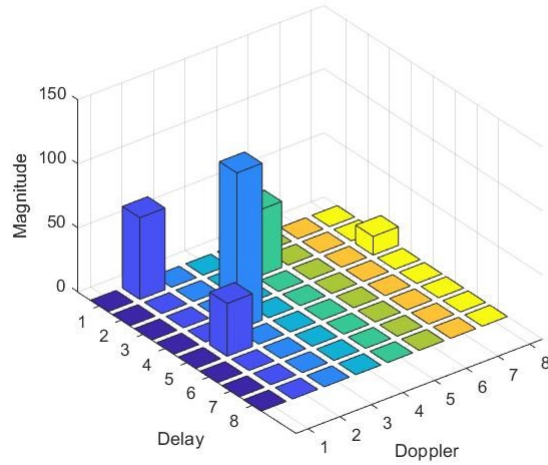


Figure 3.9: 2-D channel in the delay Doppler domain.

To get the channel in the time frequency domain we can perform the SFFT operation on the delay-Doppler channel matrix. We get the same results by substituting (3.4) in (3.10). Fig. 3.10 shows the channel in the delay-Doppler domain which is sparse in nature and Fig. 3.11 shows the corresponding time-frequency domain channel response.

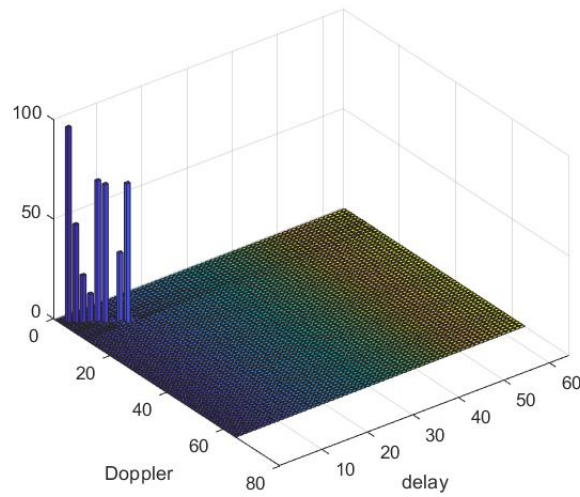


Figure 3.10: Delay-Doppler domain channel

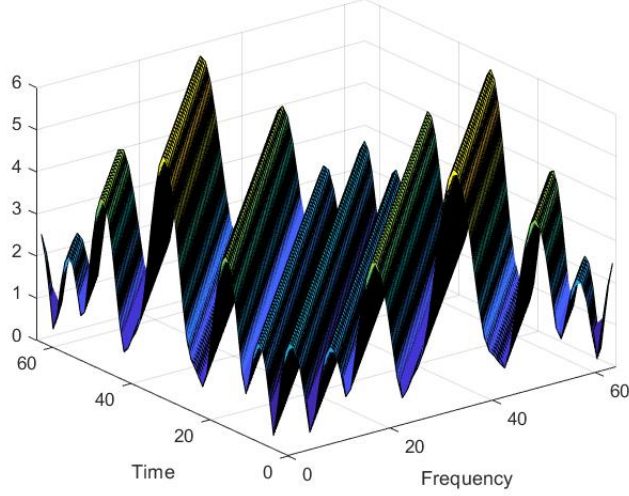


Figure 3.11: Time-frequency domain channel

Substituting (3.4) in (3.3) we get

$$r(n) = \sum_{i=1}^P h_i e^{\frac{-j2\pi k_i(n-l_i)}{NM}} s([n-l_i]_{MN}) + w(n), 0 \leq n \leq MN-1 \quad (3.19)$$

(3.19) is written in the matrix form as

$$r = H_1 s + w \quad (3.20)$$

$$H_1 = \sum_{i=1}^P h_i \Pi^{l_i} \Delta^{k_i} \quad (3.21)$$

Where  $\Pi$  is the permutation matrix and  $\Delta$  is a diagonal matrix shown below and  $h_i, l_i, k_i$  are the channel, delay and Doppler coefficients respectively.

$$\Pi = \begin{bmatrix} 0 & \cdots & 0 & 1 \\ 1 & \cdots & 0 & 0 \\ \vdots & \ddots & \vdots & \vdots \\ 0 & \cdots & 1 & 0 \end{bmatrix}_{MN \times MN}$$

$$\Delta^{k_i} = \begin{bmatrix} e^{\frac{j2\pi k_i(0)}{NM}} & \dots & \dots & 0 \\ 0 & e^{\frac{j2\pi k_i(1)}{NM}} & \dots & 0 \\ \vdots & \ddots & \ddots & \vdots \\ 0 & \dots & \dots & e^{\frac{j2\pi k_i(MN-1)}{NM}} \end{bmatrix}_{MN \times MN}$$

On simplifying (3.12) , (3.13) and (3.20) we get

$$y_{lin} = (F_N \otimes G_{rx})H_1(F_N^H \otimes G_{tx})x_{lin} + (F_N \otimes G_{rx})w \quad (3.22)$$

where

$$\begin{aligned} H_{eff} &= (F_N \otimes G_{rx})H_1(F_N^H \otimes G_{tx}) \\ \hat{w} &= (F_N \otimes G_{rx})w \\ y_{lin} &= H_{eff}x_{lin} + \hat{w} \end{aligned} \quad (3.23)$$

From (3.23) we conclude that if we know the channel matrix then we can get back the transmitted message symbols. Hence channel estimation is to be performed in order to get the channel state information (CSI). The performance of the system in decoding the transmitted symbols depends on how perfectly we are able to estimate the channel.

## CHAPTER 4

# Compressive sensing

Nyquist sampling theorem states that a sampled signal can be reconstructed without losing any information if the signal is sampled at frequency twice that of the maximum frequency of the signal. This results in too many samples which makes compression of these samples necessary before performing any operations.

Compressive sensing states that if a signal is sparse in some transformed domain, then that signal can be compressed. For example, let  $u(t)$  be a time domain signal which on sampling at Nyquist rate becomes  $u_{N \times 1}$  which is an  $N$  length vector containing samples of  $u(t)$ . According to compressive sensing if  $u$  is known to be sparse in some transformed domain say  $u = \psi x$  where  $x$  is also an  $N$  length vector which is  $K$  sparse i.e.,  $x$  has  $K$  ( $K \ll N$ ) non zero values, then  $u$  can be reconstructed from fewer samples i.e.,  $y = Au$  where  $y$  is an  $M \times 1$  vector with  $M < N$ .

$y = A\psi x = \phi x$  where  $y$  is the observation vector and  $\phi$  is the  $M \times N$  dictionary matrix. Obtaining  $x$  from  $y$  and  $\psi$  can be seen as solving an undetermined system with  $M$  equations and  $N$  unknowns ( $M < N$ ). We can recover  $x$  by  $l_0$  minimization i.e.,  $\underset{x}{\operatorname{argmin}} \|x\|_0$  subject to the constraint that  $y = \psi x$ . This is a convex optimization problem which is NP-hard.  $\|x\|_0$  is defined as total number of non-zero elements present in  $x$ . Alternatively, we use  $l_1$  minimization or greedy algorithms.  $l_1$  is defined as

$$\|x\|_1 = \sum_{i=1}^N |x_i|$$

In order to get perfect reconstruction, the dictionary matrix  $\phi$  has to satisfy the Restricted Isometry Property (RIP).

A matrix  $\psi$  is said to satisfy the RIP of order  $K$  if there exists a Restricted Isometry Constant  $\delta_k \in (0, 1)$  such that

$$1 - \delta_k \leq \frac{\|\phi x\|_2^2}{\|x\|_2^2} \leq 1 + \delta_k$$

The constant  $\delta_k$  is taken as the smallest number from  $(0, 1)$  for which the RIP is satisfied.

Compressive sensing algorithms try to find the sparse estimation of the original signal using the compressive measurements and the dictionary matrix. One of the methods is the greedy approach, which is a step-by-step iterative method. In each iteration the solution is updated by selecting those columns of the dictionary matrix which are highly correlated with the measurement vector and adding them to the support set. A few greedy algorithms discussed in this book are OMP (Orthogonal Matching Pursuit), gOMP (Generalized Orthogonal Matching Pursuit), OLS (Orthogonal Least Square) and gOLS (Generalized Orthogonal Least Square) algorithms.

All the mentioned algorithms have the same steps which are the initialization step, identifying step and the updating step. In the initialization step an  $M \times 1$  vector  $r$  called the residue vector is initialized to the measurement vector  $y$ , support set  $\Lambda$  is initialized as a null set ( $\emptyset$ ) and the solution vector  $x$  is initialized to 0. In the identifying step the atom which is to be added to the support set is calculated. In the updating step the solution vector  $x$  is updated using the least square method and the residue is calculated using the updated solution vector.

---

**Algorithm 1** OMP Algorithm [9]

---

**Input:**  $\phi, y, \text{stopping criterion}$

**Initialize:**  $r^0 = y, x^0 = 0, \Lambda = \emptyset, l = 0$

**while** *Not converged* **do**

**Match :**  $h^l = \phi^T r^l$

**Identify :**  $\Lambda^{l+1} = \Lambda^l \cup \underset{j}{\operatorname{argmax}} \|h^l(j)\|$

**Update:**  $x^{l+1} = \underset{z: \operatorname{supp}(z) \subseteq \Lambda^{l+1}}{\operatorname{argmin}} \|y - \phi z\|_2$

$r^{l+1} = y - \phi x^{l+1}$

$l = l + 1$

**end**

**Result :**  $\hat{x} = x^l = \underset{z: \operatorname{supp}(z) \subseteq \Lambda^l}{\operatorname{argmin}} \|y - \phi z\|_2$

---

---

**Algorithm 2** gOMP Algorithm [10]

---

**Input:**  $\phi, y, \text{stopping criterion}$ **Initialize:**  $r^0 = y, x^0 = 0, \Lambda = \emptyset, l = 0, n$ **while** *Not converged* **do**    **Match :**  $h^l = \phi^T r^l$     **Identify :**  $\alpha_k = \underset{j_k}{\operatorname{argmax}} \|h^l(j_k)\|$      $\Lambda^{l+1} = \Lambda^l \cup \{\alpha_1, \alpha_2, \dots, \alpha_N\}$     **Update:**  $x^{l+1} = \underset{z: \operatorname{supp}(z) \subseteq \Lambda^{l+1}}{\operatorname{arg min}} \|y - \phi z\|_2$      $r^{l+1} = y - \phi x^{l+1}$      $l = l + 1$ **end****Result :**  $\hat{x} = x^l = \underset{z: \operatorname{supp}(z) \subseteq \Lambda^l}{\operatorname{arg min}} \|y - \phi z\|_2$ 

---

The difference between the OMP and gOMP algorithms is in the identify step where in OMP we select the maximum element where as in the gOMP algorithm we select the 'n' maximum elements instead of one in each iteration.

---

**Algorithm 3** OLS Algorithm [11]

---

**Input:**  $\phi, y, \text{stopping criterion}$ **Initialize:**  $r^0 = y, x^0 = 0, \Lambda = \emptyset, l = 1$ **while** *Not converged* **do**    **Identify :**  $i_{\max} = \underset{i}{\operatorname{arg min}} \|y - \phi_{\Lambda^l} \phi_{\Lambda^l}^+ y\|_2$     **Update:**  $\Lambda^l : \Lambda^l = \Lambda^{l-1} \cup i_{\max}$      $x^l = \phi_{\Lambda^l}^+ y$      $r^l = y - \phi x^l$      $l = l + 1$ **end****Result :**  $\hat{x} = x^{l-1} = \underset{z: \operatorname{supp}(z) \subseteq \Lambda^{l-1}}{\operatorname{arg min}} \|y - \phi z\|_2$ 

---

---

**Algorithm 4** gOLS Algorithm [12]

---

**Input:**  $\phi, y, \text{stopping criterion}$

**Initialize:**  $r^0 = y, x^0 = 0, \Lambda = \emptyset, l = 1, N$

**while** *Not converged* **do**

**Identify:**  $i_{max} = \arg \min_{\Lambda^l : \Lambda^l = \Lambda^{l-1} \cup i} \|y - \phi_{\Lambda^l} \phi_{\Lambda^l}^\dagger y\|_2$

**Update:**  $\Lambda^l : \Lambda^l = \Lambda^{l-1} \cup \{i_{max1}, i_{max2}, \dots, i_{maxN}\}$

$x^l = \phi_{\Lambda^l}^\dagger y$

$r^l = y - \phi x^l$

$l = l + 1$

**end**

**Result:**  $\hat{x} = x^{l-1} = \arg \min_{z: \text{supp}(z) \subseteq \Lambda^{l-1}} \|y - \phi z\|_2$

---

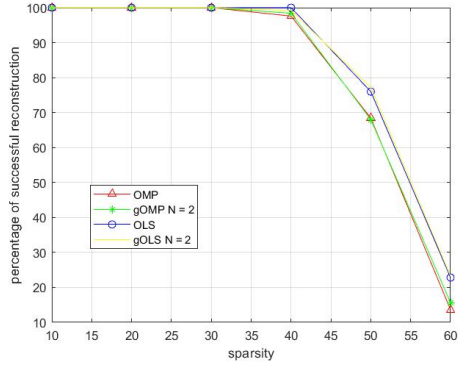
$\phi_{\Lambda^l}^\dagger$  is the Morse pseudo inverse of  $\phi_{\Lambda^l}$  which is similar to the least square solution.

OLS and gOLS algorithms differ in the same way as OMP and gOMP differ from each other that is selecting  $n$  minimum elements in gOLS instead of one in each iteration for the OLS algorithm. OPM and OLS algorithms differ in the identifying step as the OMP algorithm selects the atom which has the maximum correlation between the column of the dictionary matrix and the residue vector. Where as in the OLS algorithm the atom which has the least square error of the residue vector.

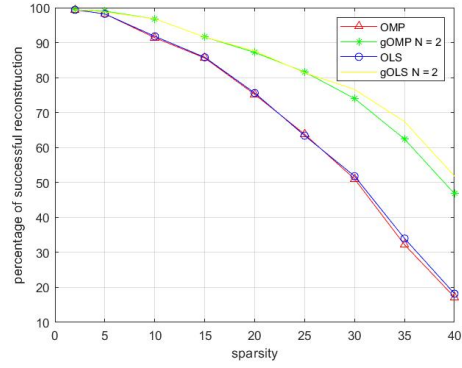
The performance of the CS algorithms depends on the sparsity of the vector which is to be reconstructed. As the sparsity order increases i.e., the non-zero elements increase the reconstruction of the sparse vector becomes difficult. This is seen in the performance analysis of the CS algorithms where we plot the percentage of successful reconstruction against the sparsity. The results are presented in Fig. 4.1 and for this we consider a  $M \times N$  ( $128 \times 256$ ) dictionary matrix  $\phi$  whose elements are gaussian distribution  $\mathcal{N}(0, \frac{1}{M})$  The  $K$ -sparse vector has the non-zero elements from either gaussian signal or randomly selected from PAM signals  $\{\pm 1, \pm 3\}$ .

In Fig. 4.2 we present the time taken by each CS algorithm for successful reconstruction as a function of sparsity. The time taken for the OMP and gOMP algorithms is less when compared to OLS and gOLS algorithms as they are less complex and the time taken increases as sparsity increases.

In Fig. 4.3 we present the iterations taken by each CS algorithm for successful reconstruction as a function of sparsity. In both figures 4.3a and 4.3b, the iterations taken by the CS algorithm increase linearly with the increase of sparsity.

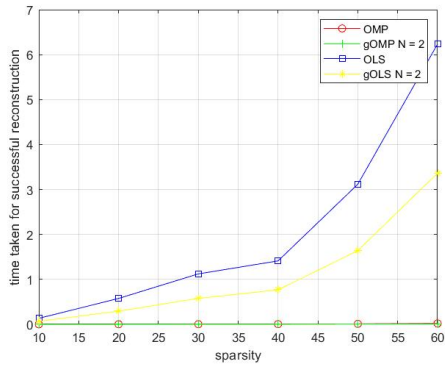


(a) PAM Signal

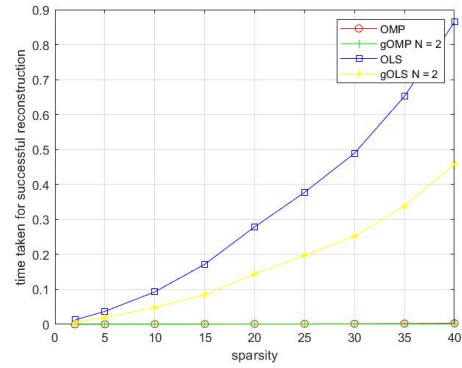


(b) Gaussian Signal

Figure 4.1: Percentage of successful reconstruction by CS algorithms as a function of sparsity

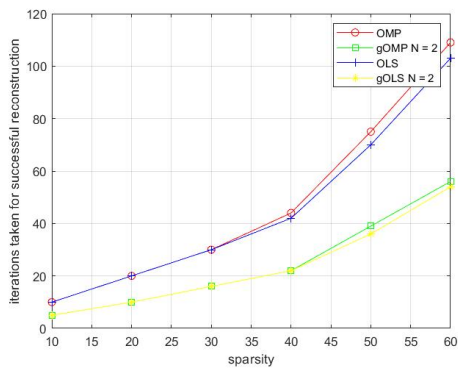


(a) PAM Signal

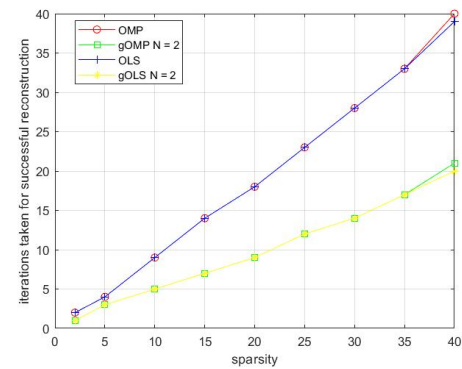


(b) Gaussian Signal

Figure 4.2: Time taken for successful reconstruction by CS algorithms as a function of sparsity



(a) PAM Signal



(b) Gaussian Signal

Figure 4.3: Iterations taken for successful reconstruction by CS algorithms as a function of sparsity



## CHAPTER 5

# Delay Doppler channel estimation

The channel in the delay-Doppler domain is sparse in nature so the compressive sensing algorithms can be applied to estimate the delay-Doppler channel. In order to apply the compressive sensing algorithms, we rewrite the OTFS system model equations in an alternate form of  $y = \phi x$  where  $y$  is the output vector and  $\phi$  is the dictionary matrix and  $x$  is the sparse input vector.

From (3.14) we can see that the input-output relation in the delay-Doppler domain is the 2D convolution with the channel matrix and the input delay-Doppler matrix. (3.14) is rewritten as

$$y_{lin} = \frac{1}{MN} H x_{lin} \quad (5.1)$$

Proof is in Appendix B.

Similarly (3.14) can also be rewritten in the form of  $y = \mathbf{X}h$  where  $h$  is  $MN \times 1$  channel vector obtained by the vectorization of the  $M \times N$  delay-Doppler channel matrix and  $\mathbf{X}$  is the  $MN \times MN$  2D matrix and  $y$  is the corresponding  $MN \times 1$  output vector. Now the 1D channel matrix  $h$  becomes the sparse vector which is to be estimated using output vector  $y$  and the dictionary matrix  $\mathbf{X}$  as the inputs for the compressive sensing algorithms.

In the Fig. 5.1 we take an example for 2D convolution of  $2 \times 2$  matrices, first element of the output  $y = y_{00}$  is obtained by the dot product of vectors  $\begin{bmatrix} 1 & 2 & 3 & 4 \end{bmatrix}$  and  $\begin{bmatrix} a & b & c & d \end{bmatrix}$  and the second element  $y_{01}$  is obtained by the dot product of vectors  $\begin{bmatrix} 1 & 2 & 3 & 4 \end{bmatrix}$  and  $\begin{bmatrix} b & a & d & c \end{bmatrix}$ , the third element of  $y$  is obtained by the dot product of vectors  $\begin{bmatrix} 1 & 2 & 3 & 4 \end{bmatrix}$  and  $\begin{bmatrix} c & d & a & b \end{bmatrix}$ , finally the fourth element of  $y = y_{11}$  is obtained by the dot product of vectors  $\begin{bmatrix} 1 & 2 & 3 & 4 \end{bmatrix}$  and  $\begin{bmatrix} d & c & a & b \end{bmatrix}$ . These dot products are written in the form of  $y = \mathbf{X}h$ . The mathematical equations are similar to the steps followed in converting (3.14) to (5.1).

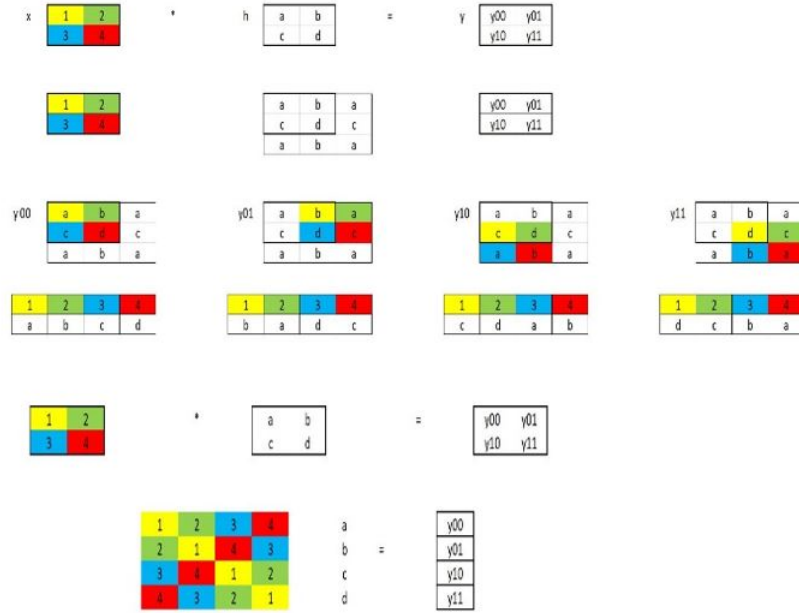


Figure 5.1: Matrix representation of the 2D convolution.

$$y[k', l'] = \frac{1}{MN} \sum_{k_2=0}^{N-1} \sum_{l_2=0}^{M-1} h_w[k_2, l_2] x[(k' - k_2)_N, (l' - l_2)_M] \quad (5.2)$$

and hence the double summation is written as a matrix equation as

$$y = \frac{1}{MN} \mathbf{X}h \quad (5.3)$$

For the DD channel estimation,  $\mathbf{X}$  is the dictionary matrix which has the modulated symbols known to both the transmitter and the receiver i.e., pilot symbols. We use the entire  $M \times N$  grid to transmit the pilots for channel estimation. In this method the first grid contains the pilot symbols for the channel estimation and once the channel is estimated we send the data symbols and use the estimated channel while decoding the data symbols at the receiver.

This method assumes that the channel remains static, so that once estimated it can be used for decoding at the receiver. This is not the case in practice as the channel is not static and changes with time. Hence, we have to design a grid which has both the pilot as well as the data symbols for transmission so that we can estimate the channel for the respective grids.

## CHAPTER 6

# Grid Design

From Fig. 3.9 and Fig. 3.10 for an  $M$  channel matrix the channel quotients are present inside a sub-matrix of size max delay spread ( $l_{max}$ ) along the Delay axis and max Doppler spread ( $k_{max}$ ) along the Doppler axis and the remaining elements of the matrix are zeros.

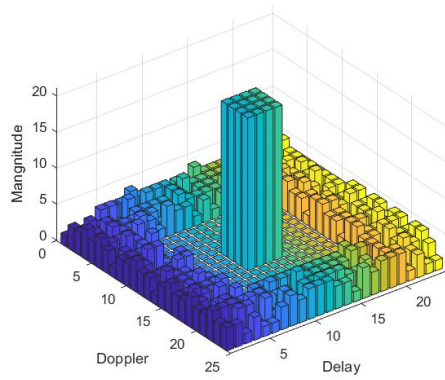
From this observation we can use a pilot grid of the size  $l_{max} \times k_{max}$  and still perform channel estimation. Hence, we design our grid such that it has pilot grid of sufficient size at the centre surrounded by a guard band then the remaining elements can be used for data transmission.

For an  $M \times N$  grid the centre ( $\frac{M}{2} - k_{max}$  to  $\frac{M}{2} + k_{max}$ ) along the Doppler axis and ( $\frac{N}{2} - l_{max}$  to  $\frac{N}{2} + l_{max}$ ) along the delay axis will be the pilot symbols grid used for CS dictionary matrix.

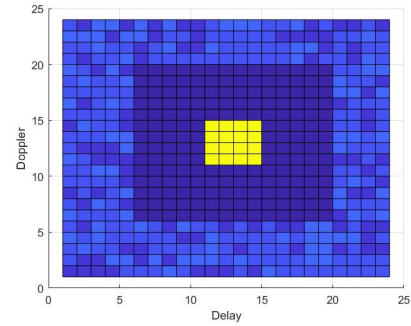
The guard band encircles the pilot grid with guard length of  $d = \max(l_{max}, k_{max})$ . Hence, the dimensions of the guard band along the delay axis ( $\frac{N}{2} - l_{max} - d$  to  $\frac{N}{2} - l_{max}$ ) and ( $\frac{N}{2} + l_{max}$  to  $\frac{N}{2} + l_{max} + d$ ) and along the Doppler axis ( $\frac{M}{2} - k_{max} - d$  to  $\frac{M}{2} - k_{max}$ ) and ( $\frac{M}{2} + k_{max}$  to  $\frac{M}{2} + k_{max} + d$ ). Rest of the  $M \times N$  grid contains the data symbols.

From Fig. 6.1a the delay-Doppler grid has the pilots in the centre which are surrounded by the guard symbols and then the data symbols are mapped in the remaining part of the grid. The size of the pilot grid and the guard symbols depend on the max delay and Doppler spread of the channel. For example, the grid in Fig. 6.1b is of size  $24 \times 24$  and if the max delay and Doppler spread of the channel is 4 then the size of the pilot grid is  $4 \times 4$  and the guard symbols are of 5 symbols in width on each side of the pilot grid which results to a grid of  $14 \times 14$  size ( $14 = 5$  (guard symbols) +  $4$  (pilot symbols) +  $5$  (guard symbols)). The remain part of the grid has data symbols.

Fig. 6.2 gives us the channel response for the delay-Doppler grid mentioned in Fig. 6.1. From the channel response the centre part of the grid is used for estimating the channel using the CS algorithms and then the estimated channel

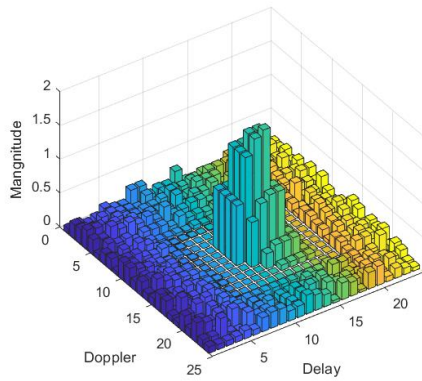


(a) Grid in 3D

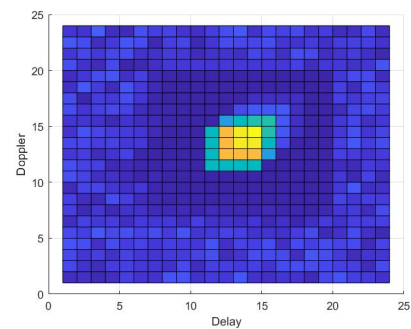


(b) Top View of grid

Figure 6.1: The delay-Doppler grid with the pilot symbols as well as the data symbols.



(a) Grid in 3D



(b) Top View of grid

Figure 6.2: The delay-Doppler channel response for the grid with the pilot symbols as well as the data symbols.

is used for estimating the data transferred in the grid. Hence this type of grid can capture the dynamic change in the channel and correspondingly modify the channel estimate for better demodulation process at the receiver side. We only consider the central position of the grid which is the pilot grid as the dictionary matrix and the corresponding central position at the receiver side as the corresponding channel output which will be given as the input parameters for the CS algorithms.

## CHAPTER 7

# OTFS-MA (Multiple Access)

We extend the OTFS system model to multiple user case scenario i.e., multiple access OTFS system (OTFS-MA) where each user has a dedicated delay slot. Consider the OTFS-MA system with  $K_u$  multiple users at the transmitter side and a single antenna to receive them. Hence at the receiver side the information from these  $K_u$  users is multiplexed on the  $M \times N$  delay-Doppler grid. The system equation (5.3) is modified as

$$y = \sum_{i=1}^{K_u} \mathbf{X}_i h_i$$

$$y = \begin{bmatrix} \mathbf{X}_1 & \mathbf{X}_2 & \cdots & \mathbf{X}_{K_u-1} & \mathbf{X}_{K_u} \end{bmatrix} \begin{bmatrix} h_1 \\ h_2 \\ \vdots \\ h_{K_u-1} \\ h_{K_u} \end{bmatrix}$$

$$\mathbf{X}_{comb} = \begin{bmatrix} \mathbf{X}_1 & \mathbf{X}_2 & \cdots & \mathbf{X}_{K_u-1} & \mathbf{X}_{K_u} \end{bmatrix}, \quad h_{comb} = \begin{bmatrix} h_1 \\ h_2 \\ \vdots \\ h_{K_u-1} \\ h_{K_u} \end{bmatrix}$$

$$y = \mathbf{X}_{comb} h_{comb} \tag{7.1}$$

Where  $\mathbf{X}_i$  is the  $MN$  data grid corresponding to the  $i^{th}$  user which is obtained by converting the  $x[k, l]M \times N$  delay-Doppler grid of the  $i^{th}$  user. For the OTFS-MA we design the grid such that each user's data does not interfere with the other user. This is done by assigning a part of the grid for single user data and the remaining part is made to zero. Below Fig. 7.1 shows the design of the delay-Doppler grid of size  $16 \times 16$  with 4 users whose data is multiplexed along the

delay axis.

$$X_u[k, l] = \begin{cases} \alpha, & \text{if } k \in \left\{ \frac{(u-1)M}{K_u}, \dots, \frac{uM}{K_u} - 1 \right\}, \quad l \in \{0, 1, \dots, N-1\} \\ 0, & \text{otherwise} \end{cases}$$

$\alpha$  is the modulated symbol.

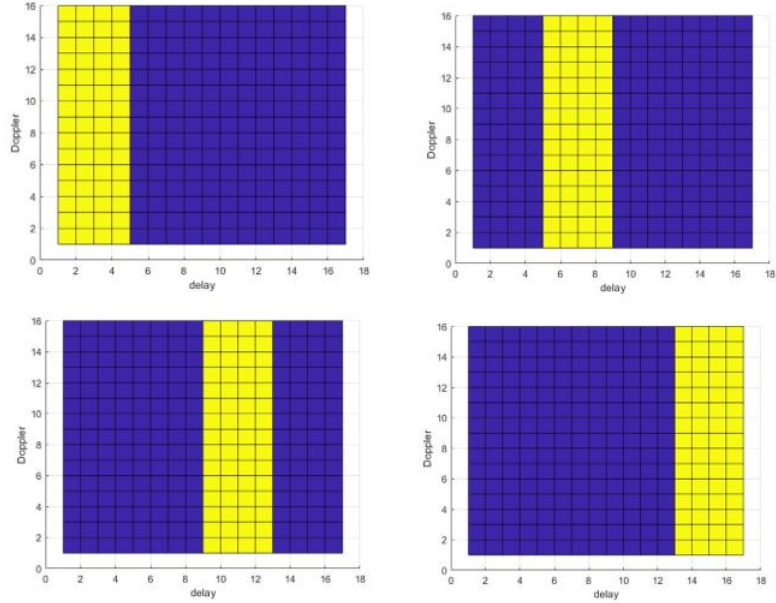


Figure 7.1: The four data grids corresponding to the 4 users in delay-Doppler domain.

Fig. 7.1 has 4 user grids and the yellow region in each user grid is the part on the grid where data of the corresponding user is transmitted. Rest of the grid is zero for the corresponding user.

## CHAPTER 8

# Results

In this section we present the performance results of the CS algorithms discussed for channel estimation. The normalized mean square error (NMSE) between the original channel ( $H$ ) and the estimated channel ( $\hat{H}$ ) from the CS algorithms as a function of noise SNR in dB scale is used.

$$NMSE = \frac{\|\hat{H} - H\|_2^2}{\|H\|_2^2}$$

A delay-Doppler grid with  $M = 4$  and  $N = 4$  with a carrier frequency of 4GHz and sub-carrier spacing of 15kHz. The channel has 4 multi-paths with a max delay spread of  $2.08 \mu s$  and max Doppler spread of 470Hz. For the channel estimation the entire grid is considered as a pilot i.e., known symbols are mapped onto the grid for transmission which are used as dictionary matrix for the CS algorithms. The results from the CS algorithms are also compared with the impulse-based channel estimation technique [2]. The noise SNR is varied from 0dB to 50dB and the NMSE performance of the estimated channel by different CS algorithms is plotted. Along with the NMSE performance we also plot the iterations taken by each algorithm and the also the time taken by each of these CS algorithms against the SNR in dB scale.



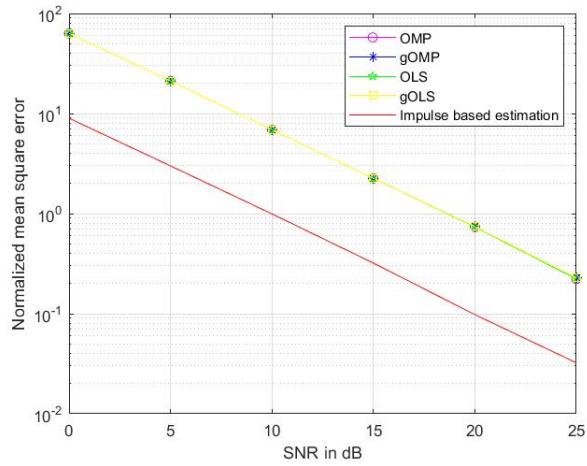


Figure 8.1: NMSE performance of OMP, gOMP, OLS, gOLS and impulse based estimation with 16 QAM symbols as the elements of the dictionary matrix.

From Fig. 8.1 we observe that the NMSE performance of the CS algorithms that are the OMP, gOMP, OLS and gOLS algorithms is same and they perform poorly when compared to the impulse-based estimation technique.

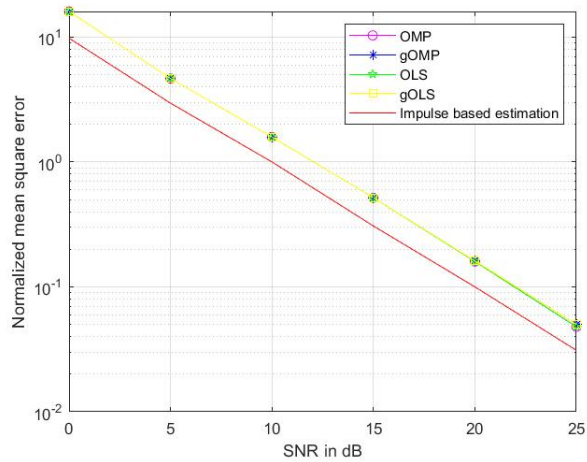


Figure 8.2: NMSE performance of OMP, gOMP, OLS, gOLS and impulse based estimation with 64 QAM symbols as the elements of the dictionary matrix.

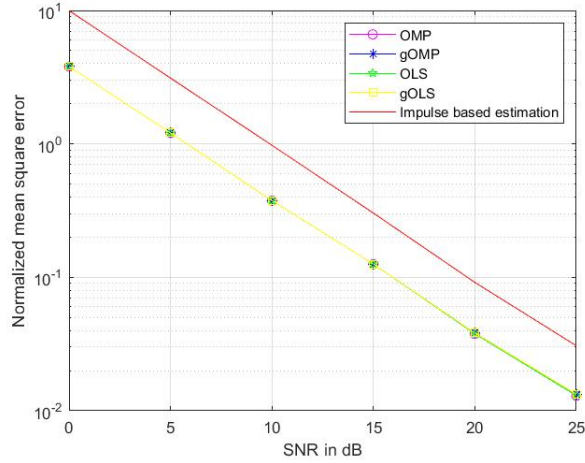


Figure 8.3: NMSE performance of OMP, gOMP, OLS, gOLS and impulse based estimation with 256 QAM symbols as the elements of the dictionary matrix.

As we increase the modulation order the performance of the CS algorithms approaches to that of the impulse based estimation technique. This is observed in Fig. 8.2 and Fig. 8.3.

In Fig. 8.4 we see the combined performance of the CS algorithms with different QAM modulation order as the elements of the dictionary matrix.

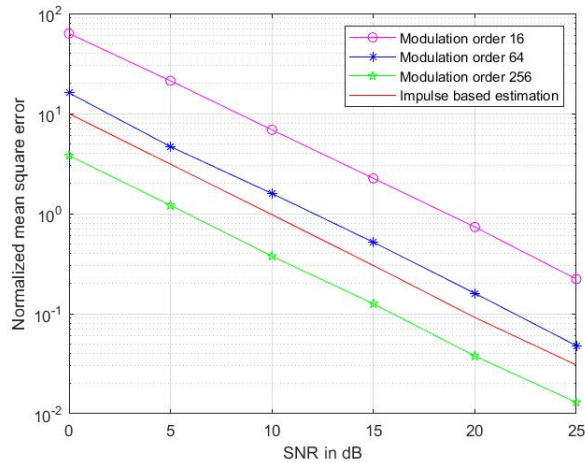


Figure 8.4: NMSE performance of OMP algorithm with dictionary matrix elements having modulation order (i)16, (ii)64, (iii)256 and Impulse based estimation.

From Fig. 8.4 we observe that as the modulation order increases the CS algorithms performance improves. This is due to the decrease in the correlation between the elements of the dictionary matrix as modulation order. The correlation of the dictionary matrix is shown in Fig. 8.5.

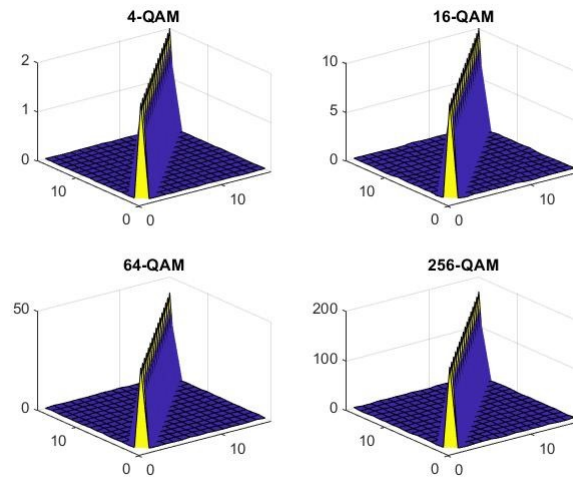


Figure 8.5: The auto correlation of the dictionary matrix with QAM symbols at different modulation order as the elements of the matrix.

To further differentiate the performance of the CS algorithms we present the number of iterations taken by each algorithm to converge as a function of the SNR in dB in Fig. 8.6 and time taken by each algorithm to converge as a function of SNR in dB in Fig. 8.7.

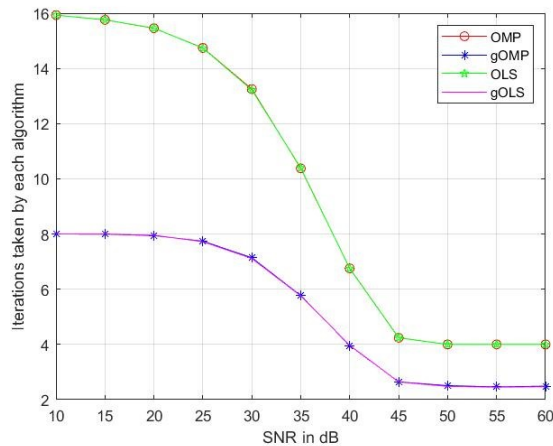


Figure 8.6: : Iterations taken by (i) OMP (ii) gOMP (iii) OLS (iv)gOLS to converge.

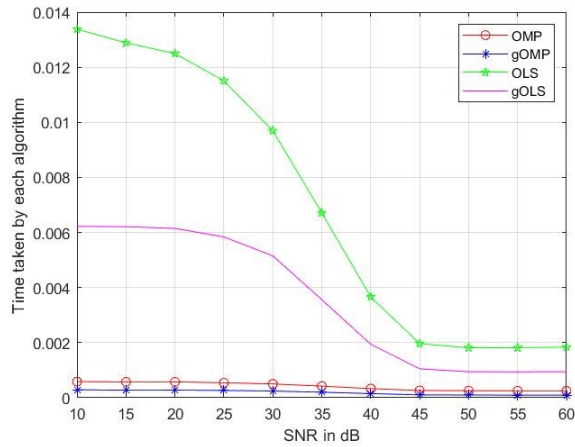


Figure 8.7: Time taken in seconds by (i) OMP, (ii) gOMP, (iii) OLS, (iv)gOLS to converge.

Fig. 8.8 shows the performance of the CS algorithms for this grid designed in Chapter 6 and they remain same as that of the previous results presented in this session.

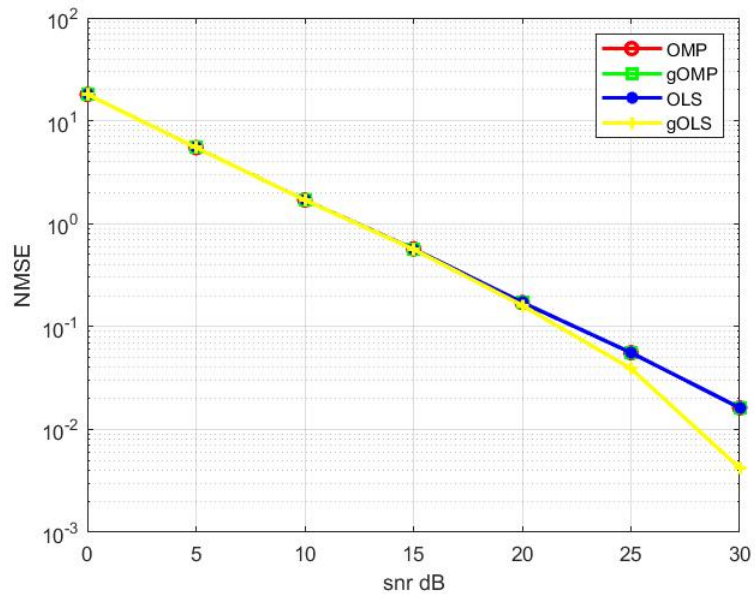


Figure 8.8: NMSE performance of OMP, gOMP, OLS, gOLS for the new grid.

Once we have the estimated channel, we perform the Least square estimation on (5.1) to get the estimated data which will be demodulated and bit error rate (BER) performance is plotted against the noise SNR in dB scale. This is shown in the Fig. 8.9.

Fig. 8.9 shows the BER performance of the estimated channel along with the BER performance when the channel is known at the receiver side.

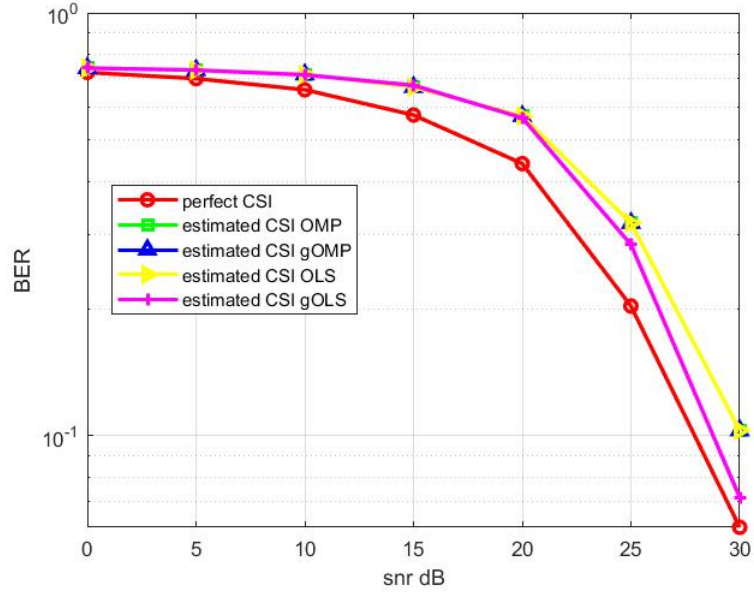


Figure 8.9: BER performance of estimated channel and when the channel is known while decoding at the receiver side.

Now we look into the performance analysis of the CS algorithms for the MA-OTFS system. The CS algorithms are applied for (7.1) and for the impulse-based estimation the grid design for each user is as shown in Fig. 8.10 and follows the below equation.

$$X_u[k, l] = \begin{cases} 1, & \text{if } k = \frac{(u-1)M}{K_u}u \in \{1, 2, \dots, K_u\}, l = 0 \\ 0, & \text{otherwise} \end{cases}$$

In the Fig. 8.10 the element marked yellow in each grid are the position where impulse is present for the 4 users and rest of the grid is zeros. The shaded region is where the corresponding user's data will be sent in the subsequent transmissions.

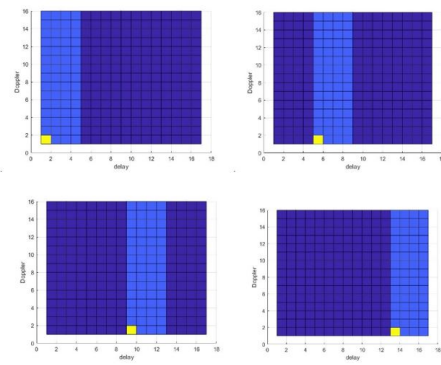


Figure 8.10: The grid design for the 4 users in the MA-OTFS case and each grid is of size 16x16.

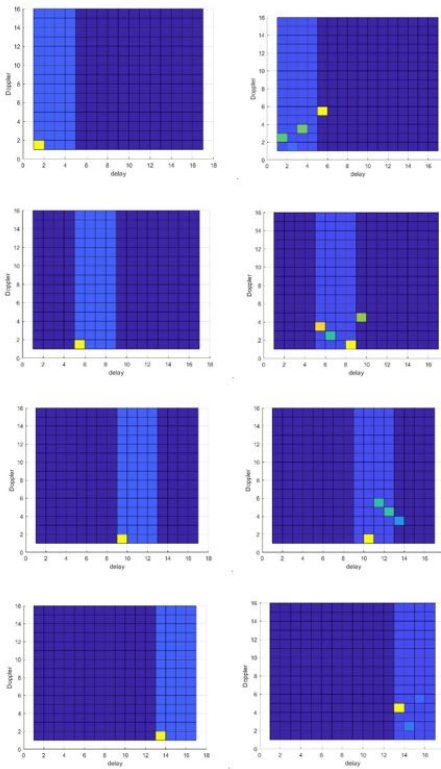


Figure 8.11: The channel response corresponding to each individual user.

The channel response for the impulse-based method is shown in Fig. 8.11. The colored elements in the grid signifies the reflectors. In the above figure the channel for each user has 4 reflectors and the reflectors have a max delay spread of 5 and max Doppler spread of 5. The 16x16 grid is divided among 4 users and each user spans 4 grid elements along the delay axis. In the channel response some of the reflectors go out of the user's allocated part in the grid this results in inter user interference when the 4 channel responses are added at the receiver side as shown in Fig. 8.12.

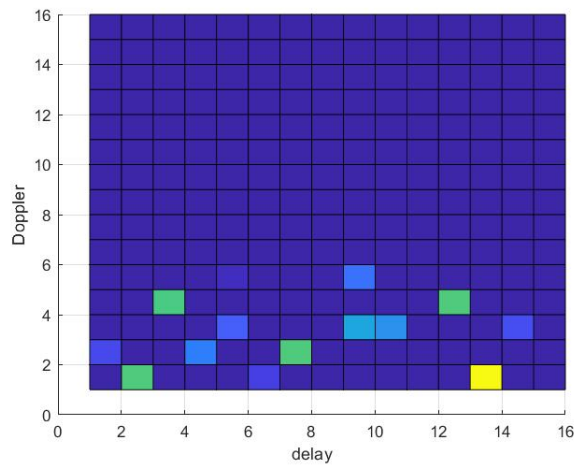


Figure 8.12: The channel response at the receiver side.

Fig. 8.13 and Fig. 8.14 shows the NMSE performance of 8x8 grid with 4 users with max delay and max Doppler spread of 2 and with max delay and max Doppler spread of 4 respectively.

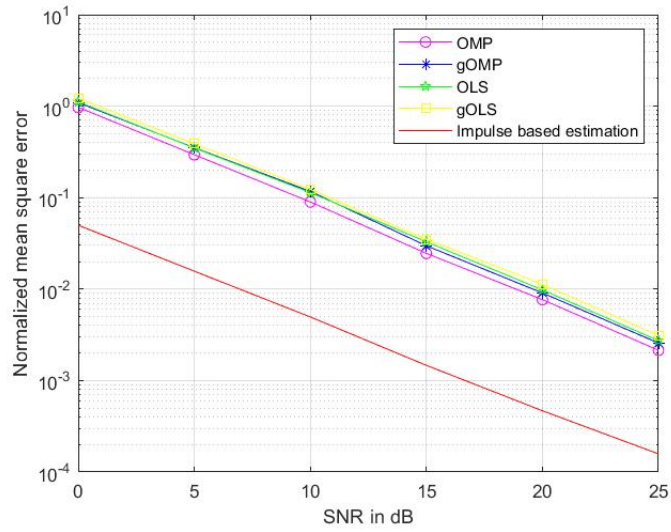


Figure 8.13: NMSE performance of 8x8 grid with 4 users with max delay and max Doppler spread of 2

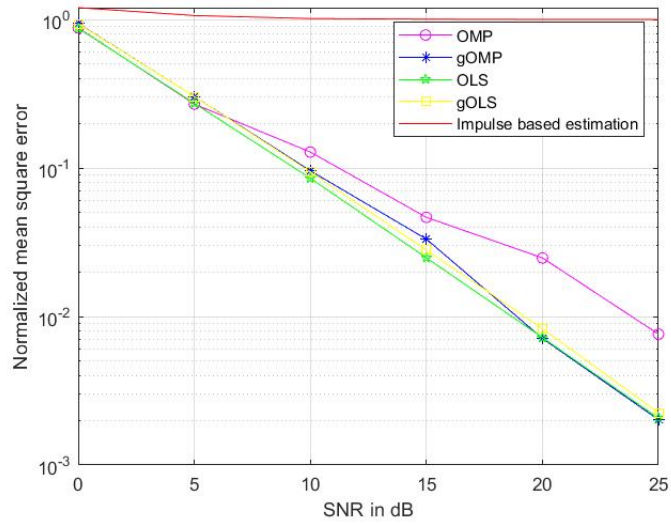


Figure 8.14: NMSE performance of 8x8 grid with 4 users with max delay and max Doppler spread of 4



## CHAPTER 9

# Conclusions

From Fig. 8.6 we observe that gOMP and gOLS take less iterations to converge because in the algorithms identifying step, we take  $N=2$  that is two max element when compared to taking only one element in the case of OMP and OLS algorithms. From Fig. 8.7 we observe that gOMP takes the least time to converge. OLS and gOLS take more time to converge than OMP and gOMP, this is because the OLS and gOLS algorithms differ from OMP and gOMP algorithms in the identifying step. The identifying step is more complex and time consuming for the OLS and gOLS algorithms.

Considering all the above mentioned results we conclude that gOMP algorithm has the better performance when compared to the other CS algorithms in estimating the DD channel.

Using the grid design as discussed in chapter 6 we can estimate the channel as well as use the grid for data transfer. Fig. 8.9 shows the BER results and We can see that the performance of the estimated channel is almost similar to that of when the channel is known at the receiver side.

The performance of CS algorithms for estimating the DD channel in the MA-OTFS case are presented in Fig. 8.13 and Fig. 8.14 and from Fig. 8.12 we can conclude that when the max delay spread is more than the elements allocated to the individual users resulting in inter user interference. This is reflected in the NMSE performance of the impulse-based estimation technique.

From Fig. 8.13 when there are 4 users (each user having 2 grid elements along the delay axis) we can see that when the max delay spread is 2 which is equal to each user's grid element along delay axis the impulse-based channel estimation has better performance than that of the CS algorithms. And in Fig. 8.14 when there are 4 users (each user having 2 grid elements along the delay axis) we can see that when the max delay spread is 4 which is greater than each user's grid element along delay axis resulting in interference and hence the CS algorithms have better performance than that of the impulse-based channel estimation.

## CHAPTER 10

# Future Scope

In Chapter 4 we discussed a few CS algorithms and were implemented in estimating the sparse DD channel. The performance of these algorithms vary from one another as seen in the results section. This opens up further opportunities to explore other algorithms which can further improve the performance in estimating the delay Doppler channel in OTFS system.

In chapter 7 we estimated the delay-Doppler channel for OTFS-MA system which is a MISO system using CS algorithms. This can be further extended to the MIMO OTFS system and see how these algorithms perform.

Similar to the grid designed in Chapter 6 a similar grid can also be designed for MISO and MIMO systems in order to estimate the dynamicaly varying DD channel .

## References

- [1] J. G. Andrews, S. Buzzi, W. Choi, S. V. Hanly, A. Lozano, A. C. K. Soong, and J. C. Zhang, "What will 5g be?" *IEEE Journal on Selected Areas in Communications*, vol. 32, no. 6, pp. 1065–1082, 2014.
- [2] A. Monk, R. Hadani, M. Tsatsanis, and S. Rakib, "OtfS - orthogonal time frequency space: a novel modulation technique meeting 5g high mobility and massive mimo challenges," 2016.
- [3] R. Hadani, S. Rakib, M. Tsatsanis, A. Monk, A. J. Goldsmith, A. F. Molisch, and R. Calderbank, "Orthogonal time frequency space modulation," *Proc IEEE WCNC 2017*, pp. 1–7, 2017.
- [4] R. Hadani and A. Monk, "OtfS: A new generation of modulation addressing the challenges of 5g," 2018.
- [5] R. Hadani, S. Rakib, S. Kons, M. Tsatsanis, A. Monk, C. Ibars, J. Delfeld, Y. Hebron, A. J. Goldsmith, A. F. Molisch, and R. Calderbank, "Orthogonal time frequency space modulation," 2018.
- [6] P. Raviteja, K. T. Phan, Y. Hong, and E. Viterbo, "Interference cancellation and iterative detection for orthogonal time frequency space modulation," *IEEE Trans. Wireless Commun.*, vol. 17, no. 10, pp. 6501–6515, 2018.
- [7] P. Raviteja, K. T. Phan, and Y. Hong, "Embedded pilot-aided channel estimation for ofts in delay-doppler channels," *IEEE Trans. Veh Tech.*, vol. 68, no. 5, pp. 4906–4917, 2018.
- [8] S. K. Mohammed, "Derivation of ofts modulation from first principles," *IEEE Transactions on Vehicular Technology*, vol. 70, no. 8, pp. 7619 – 7636, 2021.
- [9] M. A. Davenport and M. B. Wakin, "Analysis of orthogonal matching pursuit using the restricted isometry property," *IEEE Trans. Veh Tech.*, vol. 56, no. 9, 2010.

- [10] J. Wang, S. Kwon, and B. Shim, "Generalized orthogonal matching pursuit," *IEEE Transactions on Signal Processing.*, 2012.
- [11] T. Blumensath and M. E. Davies, "On the difference between orthogonal matching pursuit and orthogonal least squares," 2012.
- [12] A. Hashemi and H. Vikalo, "Sparse linear regression via generalized orthogonal least-squares," *IEEE Global Conference on Signal and Information Processing.*, 2016.

## CHAPTER A

$$y[k, l] = \frac{1}{\sqrt{NM}} \sum_{n=0}^{N-1} \sum_{m=0}^{M-1} Y[n, m] e^{-j2\pi\left(\frac{nk}{N} - \frac{ml}{M}\right)}$$

substituting  $Y[n, m] = H_{n,m}[n, m]X[n, m]$  and from (3.1)

$$\begin{aligned} &= \frac{1}{NM} \sum_{n=0}^{N-1} \sum_{m=0}^{M-1} H_{n,m}[n, m] \left[ \sum_{k'=0}^{N-1} \sum_{l'=0}^{M-1} x[k', l'] e^{j2\pi\left(\frac{nk'}{N} - \frac{ml'}{M}\right)} \right] e^{-j2\pi\left(\frac{nk}{N} - \frac{ml}{M}\right)} \\ &= \frac{1}{NM} \sum_{k'=0}^{N-1} \sum_{l'=0}^{M-1} x[k', l'] \left[ \sum_{n=0}^{N-1} \sum_{m=0}^{M-1} H_{n,m}[n, m] e^{-j2\pi nT\left(\frac{k-k'}{NT}\right)} e^{j2\pi m\Delta f\left(\frac{l-l'}{M\Delta f}\right)} \right] \\ &= \frac{1}{NM} \sum_{k'=0}^{N-1} \sum_{l'=0}^{M-1} x[k', l'] h_w[k - k', l - l'] \end{aligned}$$

where

$$h_w[k - k', l - l'] = \sum_{n=0}^{N-1} \sum_{m=0}^{M-1} H_{n,m}[n, m] e^{-j2\pi nT\left(\frac{k-k'}{NT}\right)} e^{j2\pi m\Delta f\left(\frac{l-l'}{M\Delta f}\right)}$$

And  $h_w(\tau, \nu)$  is the circular convolution of the channel response with the SFFT of the rectangular windowing function in the time-frequency domain.

$$h_w(\tau, \nu) = \sum_{n=0}^{N-1} \sum_{m=0}^{M-1} H_{n,m}[n, m] e^{-j2\pi nT\nu} e^{j2\pi m\Delta f\tau}$$

$$h_w(\tau, \nu) =$$

$$\sum_{n=0}^{N-1} \sum_{m=0}^{M-1} \left[ \int \int h(\tau', \nu') e^{-j2\pi(\nu' + m\Delta f)\tau'} e^{j2\pi\nu'nT} d\tau' d\nu' \right] e^{-j2\pi nT\nu} e^{j2\pi m\Delta f\tau}$$

$$\int \int h(\tau', \nu') \left[ \sum_{n=0}^{N-1} \sum_{m=0}^{M-1} e^{-j2\pi(\nu' - \nu)nT} e^{j2\pi(\tau - \tau')m\Delta f} \right] e^{-j2\pi\tau'\nu'} d\tau' d\nu'$$

$$\int \int h(\tau', \nu') w(\nu - \nu', \tau - \tau') e^{-j2\pi\tau'\nu'} d\tau' d\nu'$$

where

$$w(\tau, \nu) = \sum_{n=0}^{N-1} \sum_{m=0}^{M-1} 1 \cdot e^{-j2\pi(\nu nT - \tau m\Delta f)}$$

## CHAPTER B

$$y[k', l'] = \frac{1}{NM} \sum_{k=0}^{N-1} \sum_{l=0}^{M-1} x[k, l] h_w[(k - k')_N, (l - l')_M]$$

let the elements of the matrix  $y$  be known as follows:

$$y = \begin{bmatrix} y_{0,0} & y_{0,1} & y_{0,2} & \cdots & \cdots & y_{0,M-1} \\ y_{1,0} & y_{1,1} & y_{1,2} & \cdots & \cdots & y_{1,M-1} \\ \vdots & \vdots & \vdots & \cdots & \cdots & \vdots \\ y_{N-1,0} & y_{N-1,1} & y_{N-1,2} & \cdots & \cdots & y_{N-1,M-1} \end{bmatrix}_{N \times M}$$

The 2D matrix  $y$  and  $x$  are rewritten as the column vectors as follows

$$y = \begin{bmatrix} y_{0,0} \\ y_{0,1} \\ \vdots \\ y_{0,M-1} \\ y_{1,0} \\ y_{1,1} \\ \vdots \\ y_{1,M-1} \\ \vdots \\ \vdots \\ \vdots \\ y_{N-1,0} \\ y_{N-1,1} \\ \vdots \\ y_{N-1,M-1} \end{bmatrix}_{NM \times 1} \quad x = \begin{bmatrix} x_{0,0} \\ x_{0,1} \\ \vdots \\ x_{0,M-1} \\ x_{1,0} \\ x_{1,1} \\ \vdots \\ x_{1,M-1} \\ \vdots \\ \vdots \\ \vdots \\ x_{N-1,0} \\ x_{N-1,1} \\ \vdots \\ x_{N-1,M-1} \end{bmatrix}_{NM \times 1}$$

Any element of  $y$  can be obtained from the equation as

$$y[a, b] = \frac{1}{NM} \sum_{k=0}^{N-1} \sum_{l=0}^{M-1} x[k, l] h_w[(a - k)_N, (b - l)_M]$$

$$y[a, b] = \frac{1}{NM} \sum_{k=0}^{N-1} \sum_{l=0}^{M-1} x[k, l] h_w[(N - k + a)_N, (N - l + b)_M]$$

This double summation can be rewritten as

$$y[a, b] = \frac{1}{NM} h_{ab} x$$

Where  $h_{ab}$  is  $1 \times MN$  row vector and  $x$  is the column vector.

$$h_{a,b} = \begin{bmatrix} h_w[(N - 0 + a)_N, (M - 0 + b)_M] \\ h_w[(N - 0 + a)_N, (M - 1 + b)_M] \\ \vdots \\ h_w[(N - 0 + a)_N, (M - (M - 1) + b)_M] \\ h_w[(N - 1 + a)_N, (M - 0 + b)_M] \\ h_w[(N - 1 + a)_N, (M - 1 + b)_M] \\ \vdots \\ h_w[(N - 1 + a)_N, (M - (M - 1) + b)_M] \\ \vdots \\ \vdots \\ \vdots \\ h_w[(N - (N - 1) + a)_N, (M - 0 + b)_M] \\ h_w[(N - (N - 1) + a)_N, (M - 1 + b)_M] \\ \vdots \\ h_w[(N - (N - 1) + a)_N, (M - (M - 1) + b)_M] \end{bmatrix}^T \quad H = \begin{bmatrix} h_{0,0} \\ h_{0,1} \\ \vdots \\ h_{0,M-1} \\ h_{1,0} \\ h_{1,1} \\ \vdots \\ h_{1,M-1} \\ \vdots \\ \vdots \\ \vdots \\ h_{N-1,0} \\ h_{N-1,1} \\ \vdots \\ h_{N-1,M-1} \end{bmatrix}_{NM \times NM}$$

We generate a 2D matrix  $H$  of dimensions  $MN \times MN$  whose rows are the  $h_{ij}$  such that we can rewrite the double summation equation (12) as

$$y = \frac{1}{NM} Hx$$



Equation (12) can be rewritten as

$$y[k', l'] = \frac{1}{NM} \sum_{k_2=0}^{N-1} \sum_{l_2=0}^{M-1} x[k_2, l_2] h_w[(k_2 - k')_N, (l_2 - l')_M]$$

and hence the double summation is written as a matrix equation as

$$y = \frac{1}{NM} Xh$$